

An Investigation into the Stiffness Response of Lattice Shapes under Various Loading
Conditions

by

Raghav Sharma

A Thesis Presented in the Partial Fulfillment
of the Requirement for the Degree
Masters in Science

Approved June 2019 by the
Graduate Supervisory Committee

Dhruv Bhate, Chair

Jay Oswald

Beomjin Kwon

ARIZONA STATE UNIVERSITY

August 2019

ABSTRACT

One of the fundamental aspects of cellular material design is cell shape selection. Of particular interest is how this selection can be made in the context of a realistic three-dimensional structure. Towards this goal, this work studied the stiffness response of periodic and stochastic lattice structures for the loading conditions of bending, torsion and tension/compression using commercially available lattice design optimization software. The goal of this computational study was to examine the feasibility of developing a ranking order based on minimum compliance or maximum stiffness for enabling cell selection. A study of stochastic shapes with different seeds was also performed. Experimental compression testing was also performed to validate a sample space of the simulations. The findings of this study suggest that under certain circumstances, stochastic shapes have the potential to generate the highest stiffness-to-weight ratio in the test environments considered.

ACKNOWLEDGMENTS

I would like to take this opportunity to thank my master's thesis advisor Dr. Dhruv Bhate, who gave me this opportunity to work on such a creative and insightful work of research. Under his guidance, I learnt the fundamentals of the research process which has now made me capable of carrying out independent research which will be helpful in the future. Through him I got to learn first-hand how important the word 'why' is in research and it is in the anomalies that something exciting is always hiding. I would also like to thank him for being patient and motivating whenever the project wasn't moving forward in a desirable manner and I was doubting my abilities.

I would also like to thank my Mother, Father and the rest of the family for cheering me and motivating me throughout this journey. I would also like to thank the members of my research group, Irving Ramirez Chavez, Dhiraj Patil, Cameron Noe, Mandar Shinde, and Paul Paradise who were always there to help me out whenever I needed help with my research and also created an overall motivating environment which only made the completion of this project much easier.

I would like to acknowledge nTopology, who provided me a free license of their Element software for an unlimited period of time, which forms the backbone of this research.

Last, but not the least, I would like to thank Dr. Bhate for funding this research and providing financial support during my MS degree.

TABLE OF CONTENTS

	Page
LIST OF FIGURES	VI
INTRODUCTION	1
Motivation for Cellular Material Design.....	1
Four Questions in Cellular Material Design	4
What is (are) the optimum unit cells?.....	4
How should the size of the cells vary spatially?.....	5
What are the optimal cell parameters?	7
How Best Should Cells be Integrated in the larger form?.....	7
Unit Cell Selection Approaches	7
Analytical Approaches	8
Empirical Approaches	15
METHODS	20
Response Metrics	20
Bending.....	20
Tension	22
Torsion.....	23
SIMULATION SETUP.....	24
Stochastic lattices	33

	Page
Simulation for beam bending case	35
Simulation for tensile loading case	36
Simulation of Torsional Case	39
Manufacturing of lattice specimen for Experimental Tests	38
Compression Testing of Specimens	42
RESULTS	44
Bending Load Case	44
Tensile Load Case	49
Observations for Torsional Loading Case	54
Reproducibility of Simulation Results	58
Compression Testing (Experimental)	60
DISCUSSION	63
Periodic Case: Bending	63
Periodic Case: Tension	64
Periodic Case: Torsion	65
Stochastic Case: Bending	66
Stochastic Case: Tension	67
Stochastic Case: Torsion	67
Effect of Node Thickness	70

	Page
LIMITATIONS.....	72
CONCLUSIONS AND FUTURE WORK.....	73
BIBLIOGRAPHY	75

LIST OF FIGURES

Figure	Page
1- Ashby Plot for strength versus density for materials available in the contemporary world (Fleck, Deshpande, and Ashby 2010).....	1
2- Classification of unit cell shapes as proposed by Bhate et al. (Bhate et al. 2019)	5
3- Four Questions in Cellular Material Design (Bhate et al. 2019)	6
4(a), 4(b)- Stress-Strain characteristics of different deformation mechanisms adapted from (Ashby, 2006).....	10
5- Explanation of Maxwell Stability Criterion with a 2D pin-joint frame	11
6- This ring assembly satisfies Maxwell criterion but is found to be statically and kinematically indeterminate (Pallegirino and Calladine 1986).....	13
7- Example of a cube edge being subjected to compression loading	16
8- Properties of a hexagonal honeycomb being established for compression loading (Sharma et al. 2018).....	17
9- Commercial computational tools for lattice design optimization broadly fall into three categories	20
10- Imported geometry with chosen lattice shape and rule	26
11- Lattice Tessellation of Imported Geometry	25
12- Classification of chosen cell shapes on basis of tessellation	27
13- Selection objects in Element analysis tool	29
14- Constraints for structural loading applications	30
15- Add load toolbox	30
16- Application of boundary conditions and forces for symmetric bending case	31
17- Element analysis solution setup.....	33

Figure	Page
18- Sample solution of symmetric bending problem.....	32
19- Object info result to calculate volume of thickened lattice	33
20- Stochastic lattice generation	34
21- Symmetric bending load case with applied load and constraints	35
22- Tension load-case with applied load and constraints	36
23- Torsion load case with applied load and constraint.....	37
24- Effect of number of cells for determining mechanical properties (Le et al. 2017). ...	38
25 (a),(b),(c),(d) – CAD files of testing specimen of Cube Edge, Hex Prism Vertex Centroid, Tet Oct Vertex Centroid and Stochastic Seed-61 respectively	41
26 - Instron 8801 Servohydraulic Mechanical Tester at the ASU Polytechnic campus that was used in this work.....	43
27- Relative bending rigidity versus relative density plot for periodic shapes.....	44
28- Relative bending rigidity versus relative density plot and corresponding contour plots for Oct Vertex Centroid	45
29- Relative bending rigidity versus relative density plot for stochastic shapes	46
30- Relative bending rigidity versus relative density plot and corresponding contour plots for Stochastic- Seed 7	47
31- Relative bending rigidity versus relative density plot for Stochastic-Seed 7 and periodic shapes.....	48
32- Relative Young's modulus versus relative density plot for periodic shapes	49
33- Relative Young's modulus versus relative density plot and corresponding plots for Cube Edge.....	50
34- Relative Young's modulus versus relative density plot for stochastic shapes	51

Figure	Page
35- Relative Young's modulus versus relative density plot and corresponding contour plots for Stochastic- Seed 4.....	52
36- Relative Young's modulus versus relative density plot and corresponding contour plots for Stochastic- Seed 7 and periodic shapes	53
37- Relative shear modulus versus relative density plot for periodic shapes	54
38- Relative shear modulus versus relative density plot and corresponding contour plots for Cubic Diamond	55
39- Relative shear modulus versus relative density plot for stochastic shapes.....	56
40- Relative shear modulus versus relative density plot and corresponding contour plots for Stochastic- Seed 5	57
41- Relative shear modulus versus relative density plot for Stochastic-Seed 5 and periodic shapes	58
42- Stress vs strain curves for quasi-static compression after testing.....	59
43- Stress vs strain curves for quasi-static compression after testing near elastic region	60
44- Young's modulus versus relative density scatter plot for tested specimen	64
45- Relative young's modulus per unit relative density versus relative density scatter plot for the tested specimen.....	61
46- Relative young's modulus per unit relative density versus relative density scatter plot for the tested specimen.....	
..... Error! Bookmark not defined.	
47- Oct Vertex Centroid unit cell.....	63
48- Cube Edge unit cell.....	64
49- Cube Edge lattice with 1.6mm node thickness.....	64
50- Cubic Diamond unit cell.....	65

Figure	Page
51- Cubic diamond lattice subjected to torsion.....	66
52- Qualitative histogram of various shapes evaluating stiffness metric under respective load cases	69
53- No nodes after thickening of Cube Edge lattice by solver	70
54- Nodes can be seen prominently in the CAD file (left) and printed sample (right) of Cube Edge lattice	71

INTRODUCTION

Motivation for Cellular Material Design

Structural design is one of the fundamental domains of both study and application in mechanical engineering. As a field of study, it can be said to have three inter-related aspects: the material(s) selected for design (composition), the manufacturing process involved (captured in process-structure-property relationships), and how the material is distributed over the domain (geometry).

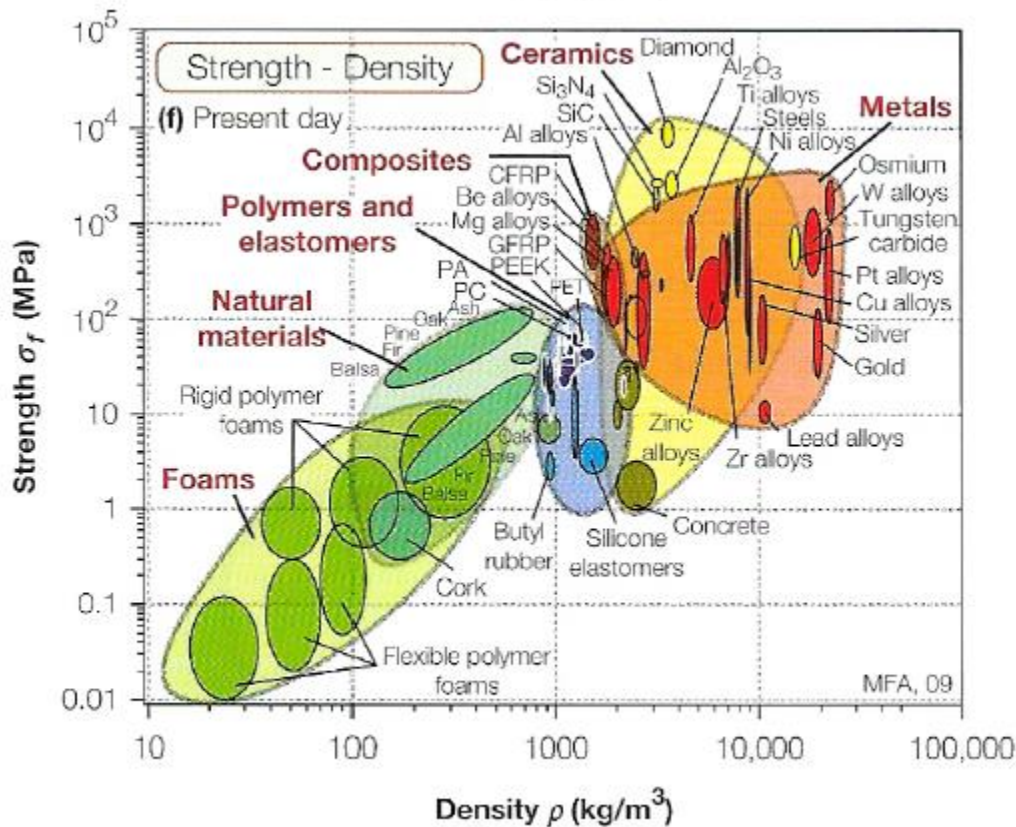


Figure 1- Ashby Plot for strength versus density for materials available in the contemporary world (Fleck, Deshpande, and Ashby 2010)

An ideal material is one which can provide the desired properties with minimum weight and cost, typically selected using an “Ashby plot” such as the one shown in Figure 1, which shows the relationship between strength and density plot several materials. This is a quantitative plot, qualifying material based on strength and weight. Similar plots exist for other material properties, such as hardness and stiffness. Over the years this library has grown from bones and animal skin to metals to carbon fibers and composites (Fleck, Deshpande, and Ashby 2010).

The most common usage of the Ashby plot involves the selection of homogeneous materials. However, there are certain applications such as helmets, which require high energy absorption to avoid injury due to impact loading and at the same time keep the weight as low as possible, where homogeneous materials may not be ideal candidates as design choices. To meet such challenges and fill gaps in the material property space represented in the plot above, one strategy is the use of cellular materials – and several “Ashby-like” plots now include these materials as well. Cellular material is an umbrella term for honeycombs, lattices and foams. The difference between lattices and foams, from a practical perspective, is the relative density of these two materials. Relative density is defined as the ratio of the density of the cellular solid and the density of the box bounding the cellular solid (Gibson & Ashby, *Cellular Solids: The mechanics of honeycombs*, 1997). For lattices, the relative density typically ranges from 0.01 to 0.3, and for foams it ranges from 0.3 to 0.5 (Gibson & Ashby, *Cellular Solids: The mechanics of honeycombs*, 1997). Lattices also tend to be beam-based structures, typically of a

periodic nature, while foams have their origin in foaming processes, which result in stochastic shapes with open and/or closed cells.

Lattice materials have become increasingly popular in the literature due to their potential to not only meet the above-mentioned requirements but also provide unique functional applications. The manufacturing of lattice materials has also been greatly enabled with the arrival of Additive Manufacturing technologies, which are now occupying several niches within the landscape of functional, production parts. One such instance is in the medical field, in particular the manufacturing of hip implants. The ball section of the hip implant which goes into the socket joint is covered with lattice geometry which not only fits well into hip-bone socket, but allows bone in-growth into the ball of the implant due to the high porosity of the lattice material (Rosen et al. 2006). Bone implants are also designed with lattices to tailor their elastic stiffness to match those of bone, which is challenging to do with homogeneous materials in the library of bio-compatible and certified materials for implantation into the human body.

One of the major limitations of working with lattice structures for structural design applications is the absence of a mathematical or simulation model that reliably captures the behavior of lattices *within three-dimensional structures* subjected to loadings such as bending, torsion and shear. Models are typically derived using homogenization methods based on empirical experimental or computational studies of simple specimens or unit cells, with limitations in their applicability to real structures with more complex stress states. The same can be said of analytical models, such as those derived from beam theory. As such, a unified model that can predict behavior in structures of real interest to

a designer is still a critical challenge (R. Sharma et al. 2018). Currently available commercial lattice design software require the designer to *a priori* specify a specific cell shape - there is no formal methodology for selecting one. This research work is dedicated to making a contribution to this specific challenge.

Four Questions in Cellular Material Design

One approach to developing a design methodology for cellular materials is to identify the important questions and then set about addressing them in the context of the application of interest (Bhate, 2019). The questions are as follows:

1. What is the optimum unit cell?
2. How should the size of the cells vary spatially?
3. What are the optimal cell parameters?
4. How best should the cells be integrated with the larger form?

What is (are) the optimum unit cells?

The first step in cellular material design, and the specific focus of this research, is choosing an optimum cell shape from the large plethora of shapes available. To make more sense of the shapes available, one may organize them so that a procedure or analysis done for one unit cell shape can be used for comparative purposes with others. One method of classifying unit cell shapes is demonstrated in figure 2 (Bhate et al. 2019). In this classification, the unit cells are grouped on the basis of their tessellation (the division of space into smaller, repeating entities), elements (the material constituents of that space), and connectivity (the ways in which these constituents are connected).

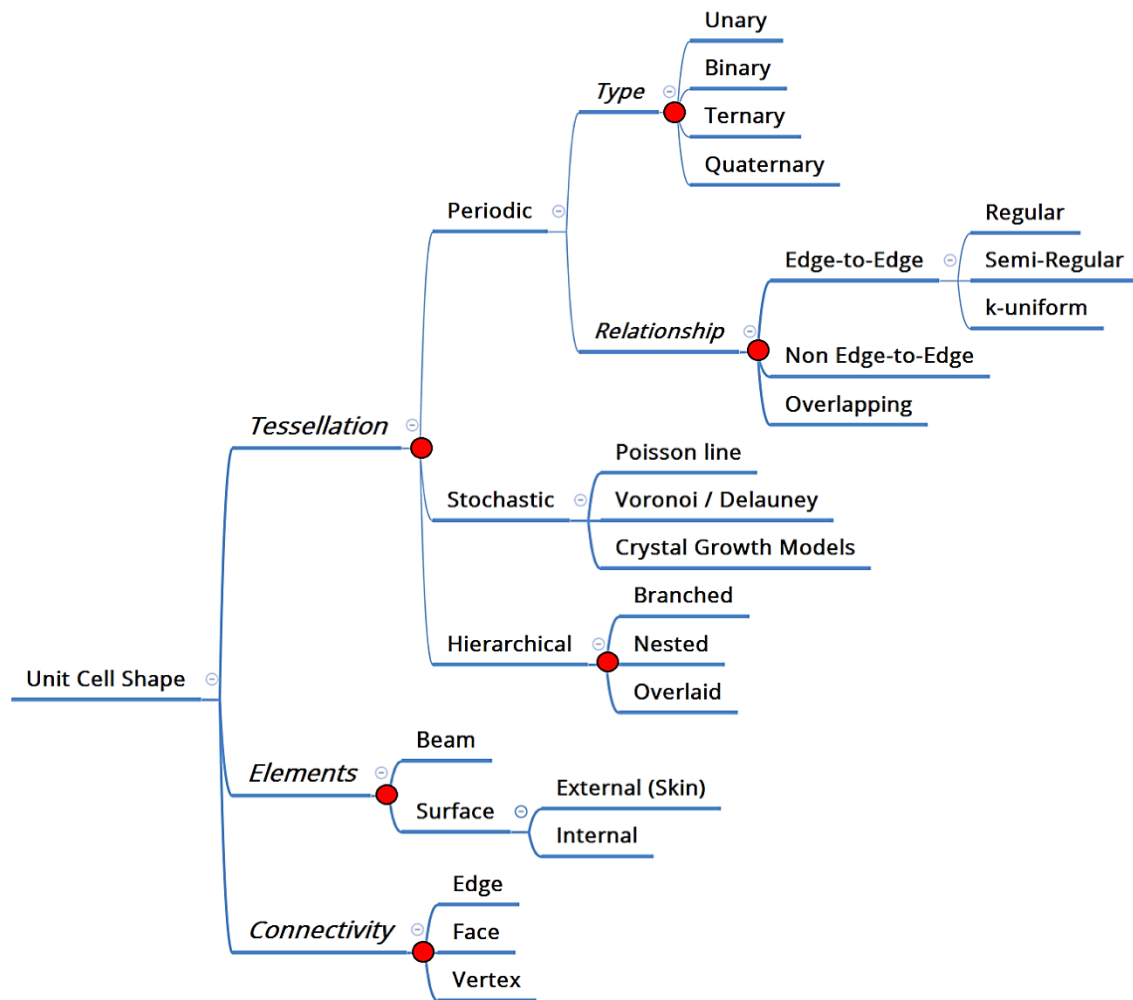


Figure 2- Classification of unit cell shapes as proposed by Bhate et al. (Bhate et al. 2019)

Tessellations can further be classified into periodic unit cells (regular unit cells repeating in all directions of the structure), stochastic (random division space following a certain law or principle such as Voronoi) and hierarchical.

How should the size of the cells vary spatially?

Once a cell shape is selected, the next factor of consideration is determining how it is to be distributed in the design space. For structural design, i.e. design with

mechanical loading considerations (as opposed to thermal or fluid considerations), regions in the structure which experience high stress, are expected to be thicker with regard to strut thickness, while regions with low stresses will be correspondingly thinner. Cell size and cell thickness are the two primary parameters that are varied to achieve relative density variation or spatial mass distribution.

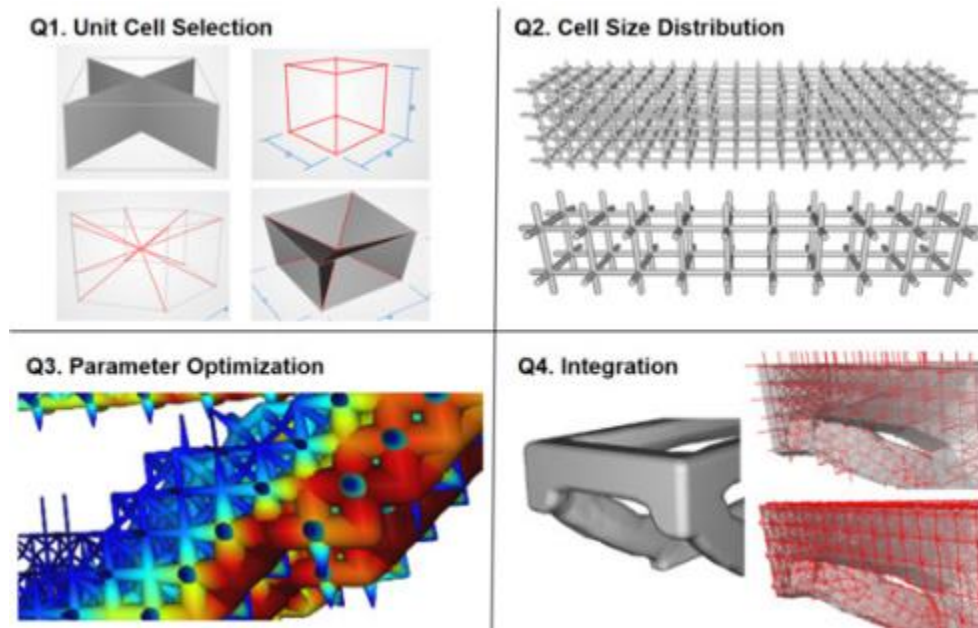


Figure 3- Four Questions in Cellular Material Design (Bhate et al. 2019)

The distribution of unit cells from a purely design point of view is governed by what unit cell has been selected and what is the application for which lattice optimization is being performed. From a manufacturing point of view, the minimum cell size that can be printed is bounded by the resolution of the manufacturing process, as well as the minimum cell size which will allow for satisfactory post-processing of the manufactured lattice. As an example relevant to this thesis work, a lattice printed with Selective Laser

Sintering (SLS), which is an additive manufacturing processes that uses polymer powder sintering as the principle technology, will have a lower bound on how small the unit cell needs to be, which is set by the laser spot diameter as well as the need to remove trapped powder after printing.

What are the optimal cell parameters?

Once the unit cell and their distribution has been determined across the structure, other unit cell parameters such corner radius and thickness are determined for optimal lattice design. This is a particular area where lattice design optimization software has come to provide value since it is possible with these software packages to modify parameters locally based on the local stresses (for structural simulation), as opposed to rely on one, globally defined optimum.

How best should cells be integrated in the larger form?

The final challenge in lattice optimization design is how the lattice integrates with the solid design space. Some options to be considered here are whether one replaces the design space with the lattice entirely, replaces only some parts with cellular material, or replaces the design space entirely with lattices and covers it with a continuous skin of solid material.

Answering these four questions is vital to designing functional and lightweight cellular structures for various loading applications. The research in this thesis focuses on answering this first, of four questions, regarding unit cell selection, and proposes a methodology for the same.

Unit Cell Selection Approaches

The shape of the unit cell of a lattice is one of the critical governing factors of the behavior of the structure when it is subjected to certain loading conditions. The loading condition imposed on the lattice can be structural (Zhu and Keller 2004), thermal (Seepersad et al. 2006), or photonic (optical) (V George et al. , 2011) in nature, depending on the application for which the lattice structure is being designed. This study is limited in scope to structural loading cases for utilization in load-bearing applications. The larger findings derived from, and methodology underlying this work are likely to be extendable to other physical domains.

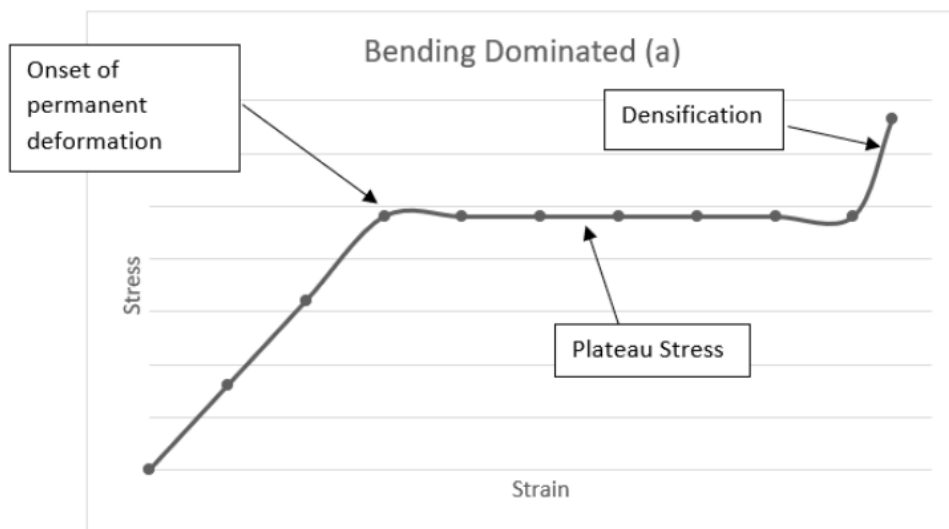
The approaches used in the literature to analyze cell shapes with the intent of selecting between different options, can be broadly speaking, broken down into two categories: the analytical, and the empirical. These are discussed in detail in the subsequent sections.

Analytical Approaches

One of the earliest approaches of predicting lattice behavior by unit cell analysis is the analytical approach, in which mathematical models are developed to predict behavior of a particular unit cell lattice shape. The major advantage of this approach is its mathematical elegance which lends to deep insights between structure and behavior. For some analytical approaches, it can also provide this insight rapidly with limited analysis and without necessitating computational tools. However, analytical models have limited applicability beyond behavior prediction for relatively simple geometries experiencing uniform loading conditions. Further, they do not typically address non-uniformities in

geometry and environment, such as multi-axial stress states, edge effects, and spatially varying cell parameters. Some analytical methods commonly used for lattices are briefly reviewed here.

A popular design approach in cellular materials is to classify shapes, purely on the basis of their geometric configuration, as stretch- or bending dominated shapes. Bending-dominated structures usually exhibit lower modulus and strength, compared to stretch-dominated structures. As can be seen from the idealized mechanical response shown in Figure 4(a), bending-dominated structures usually exhibit the classical plateau stress-strain curve. In comparison, for stretch-dominated structures, as can be seen in Figure 4(b), the initial failure of stretch-dominated structures usually occurs at higher stress levels. From an application perspective, stretch dominated structures tend to be used where structural stiffness is sought after. Bending dominated structures tend to find application where compliance and/or energy absorption at low transmitted stresses are desired.



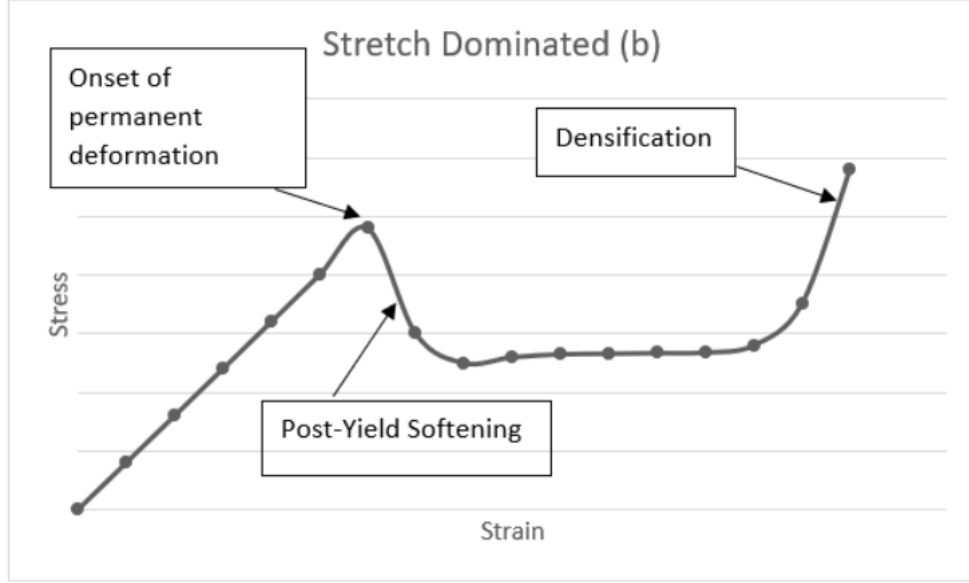


Figure 4(a), 4(b)- Stress-Strain characteristics of different deformation mechanisms adapted from (Ashby, 2006)

A classification method that is widely used to analyze the structural performance of different lattice structure shapes and classify them as stretch- or bending dominated is the Maxwell stability criterion (J.C. Maxwell, 1864). Maxwell stability criterion is assumed to be applied to a pin-jointed frame arrangement, as shown in Figure 5.

For 2D arrangements, it is given as:

$$M = b - 2j + 3 \quad (1)$$

and its 3D counterpart is expressed as:

$$M = b - 3j + 6 \quad (2)$$

where M is the Maxwell stability number, and b, j are the number of struts and joints of the framework, respectively.

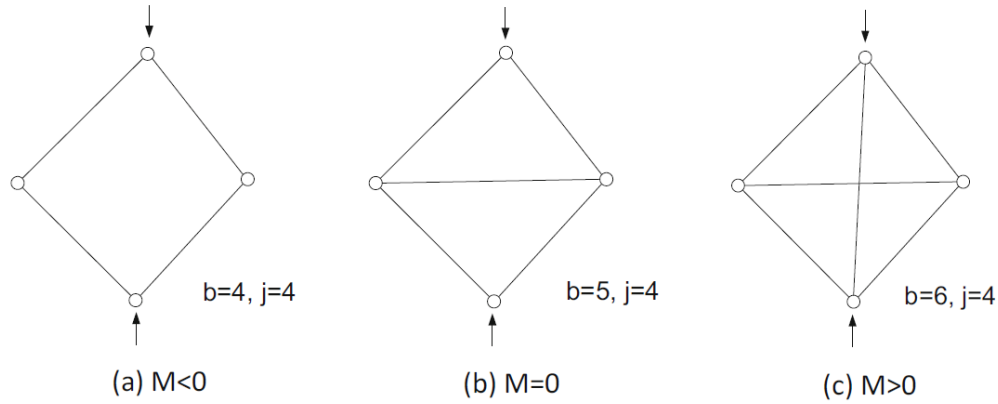


Figure 5- Explanation of Maxwell Stability Criterion with a 2D pin-joint frame

Figure 5 demonstrates distinct 2D frameworks that exhibit different Maxwell stability number. $M<0$ indicates a kinematically unstable framework system (Fig. 5a), which upon loading is unable to retain original shape or construction thereby not producing any resistance to the applied load. Such structures are *kinematically indeterminate* since the position of joints cannot be uniquely determined when the loads are applied. $M=0$ indicates a statically and kinematically determinant system with no redundancy or surplus structural members i.e. it just resists the applied load. (Fig. 5b), while $M>0$ indicates a *statically indeterminant* system (Fig. 5c), with surplus or redundant structural members, which means the structure contains extra members which removed will make no difference to the ability of the structure to resist applied load. (J.C. Maxwell, 1870)

The application of Maxwell's stability criterion to lattices, with their rigid joints, rather than pin-jointed joints is in principle problematic. However, despite that limitation,

the Maxwell criterion will determine the dominant deformation mechanism of the structure in most instances. For cellular structures with $M < 0$, the dominant deformation mechanism is strut/wall bending. For cellular structures with $M > 0$, the dominant deformation mechanism is strut/wall stretching/compressing and therefore the structure is termed stretch-dominated structure. For cellular structures with $M = 0$, a mixed deformation mode is often observed, however, the structure could still be considered to have a stretching dominated deformation mechanism since that is the pre-dominant response observed. (Deshpande, Ashby, & Fleck, 2001)

Per Calladine, Maxwell stability criterion is a necessary but not a sufficient condition for rigidity as it does not account for self-stress and hence found to be inaccurate for certain cases. For example, if the vertical strut in Fig. 5c is shortened, it pulls the other struts into compression, the compression is balanced by the tension it carries. Hence, the struts are carrying stress even though the structure carries no external loads. Figure 6 shows a configuration that satisfies the Maxwell criterion but is found to be indeterminate despite this.

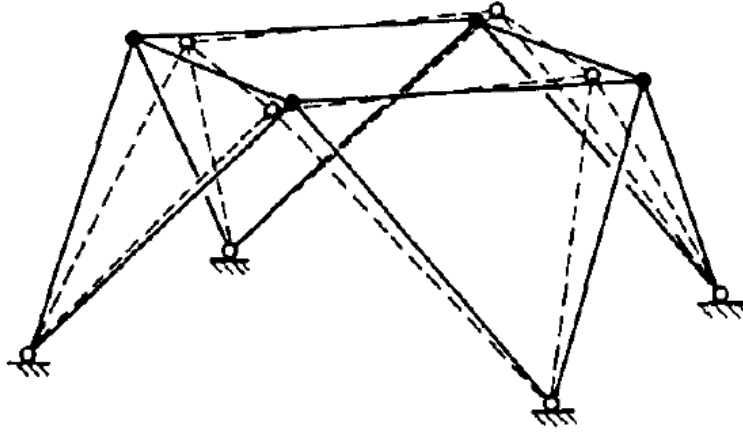


Figure 6- This ring assembly satisfies Maxwell criterion but is found to be statically and kinematically indeterminate (Pellegrino and Calladine 1986)

A more generalized form of Maxwell criterion was therefore proposed by Calladine (Pellegrino and Calladine 1986). It is stated as:

$$M = b - 3j + 6 = s - m \quad (3)$$

where s and m are the number of states of self-stress and of mechanisms respectively. For a given configuration, s is the number of modes of self-stress which means if there is one member loading the configuration with self-stress, then $s=1$, if there are two such struts $s=2$, so on and so forth. While m is the number of modes or ways in which a given configuration can move or perform motion. If there is no way or mode a mechanism can move when it is loaded, then $m=0$. If there is only one mode of movement of a given configuration then $m=1$ and so on. A method to find both the parameters is described by Pellegrino and Calladine (Pellegrino and Calladine 1986) by finding the rank of the equilibrium matrix that describes the frame in a full structural analysis. A just rigid framework has $s=m=0$. The nature of Maxwell's rule as a necessary rather than sufficient

condition is made clear by examination of the modified rule: vanishing of the left-hand side only implies that the number of mechanisms and states of self-stress are equal, not that each equal zero. If $m > 0$, then the frame contains mechanisms and will tend to collapse when loaded, therefore, it is assumed to be a bending dominated structure. If, instead, $m = 0$, then the frame ceases to be a mechanism and then such structures can be termed as stretch dominated instead.

Another approach to comparative analysis of cellular materials is the development of scaling laws based on classical beam theory as described by Ashby, Gibson and their co-workers (Gibson et al., 1997). It states that for a 3D lattice,

$$E^* = BE\rho^m \quad (4)$$

$$\sigma_y = C(\sigma_{ys})\rho^n \quad (5)$$

where B and C are proportionality constants, m and n are scaling constants, and ρ is the relative density of the lattice material. E and σ_{ys} represent the Young's modulus and yield strength, respectively, of the constitutive material of the lattice, while E^* and σ_{ys} are the corresponding value for the lattice itself. For stretch-dominated (rigid) structures, it is derived that $m=n=1$. While for bending-dominated (non-rigid) structures, it is derived that $m=2$ and $n=1.5$ (Fleck, Deshpande, and Ashby 2010).

Per Meza et al., (Meza et al. 2017b), the scaling laws discussed above are applicable for lattices which are slender, that is when $R/L < 0.05$, where R and L are the radius and length of the individual strut respectively. For non-slender beams (with $R/L \geq 0.05$), scaling laws based on beam-theory under-predict the stiffness and strength of

lattices, since nodes have a dominant effect on the stiffness of the lattice as the R/L ratio increases. Additionally, shearing and torsion effects become significant with increasing R/L ratio, which is ignored in classical stiffness models. As a result, the struts in the lattice undergo both stretching and bending mechanisms. The corrections to the scaling laws are given below:

$$E_{non-rigid} = E_s / \left(A1 \left(\frac{R}{L} \right) + A2 \left(\frac{R}{L} \right)^{-4} \right) \quad (6)$$

$$E_{rigid} = E_s * (1 + B3 \left(\frac{R}{L} \right)^{-2}) / (B1 \left(\frac{R}{L} \right)^{-2} + B2 \left(\frac{R}{L} \right)^{-4}) \quad (7)$$

Here, $A1$, $A2$, $B1$, $B2$ and $B3$ are geometry dependent constants and E_s is the modulus of the constituent material.

Empirical Approaches

Another approach of predicting lattice behavior from the unit cell is to study them empirically. In the empirical approach, the lattice structure is analyzed via computational or experimental methods to develop predictive models of the lattice composed of the unit cell. The advantage of such an approach is that it can be extended to lattice shapes that are beyond the reach of analytical models, and also not prone to the limitations described in the previous section. Empirical approaches can be expensive, in terms of computational time, or in terms of material and time costs to enable experimentation.

The most common form of extracting unit cell behavior computationally is to use Finite Element Analysis (FEA) by modeling a unit cell geometry subjected to periodic boundary conditions. From the resulting behavior of the unit cell, effective properties are

estimated under various loading conditions such as compression. This approach is computationally efficient as only the unit cell is being simulated rather than the entire lattice itself which also gives the freedom to analyze complex unit cell shapes with great ease. This approach is the most common one to predict lattice behavior owing to its ease of implementation and time required (Berger, Wadley, and McMeeking 2017), (Meza et al. 2017a). It also enables comparisons between different shapes as well as to theoretical bounds (Berger, Wadley, and McMeeking 2017). Another empirical approach to establish the effective properties of lattices is to simply manufacture the lattice and subject the lattice to the loading condition for which the lattice properties are needed, as shown in Figures 8 and 9 for different honeycombs under compression. (Meza et al. 2017a; N. Sharma, Gibson, and Ayorinde 2006; Wei et al. 2016).

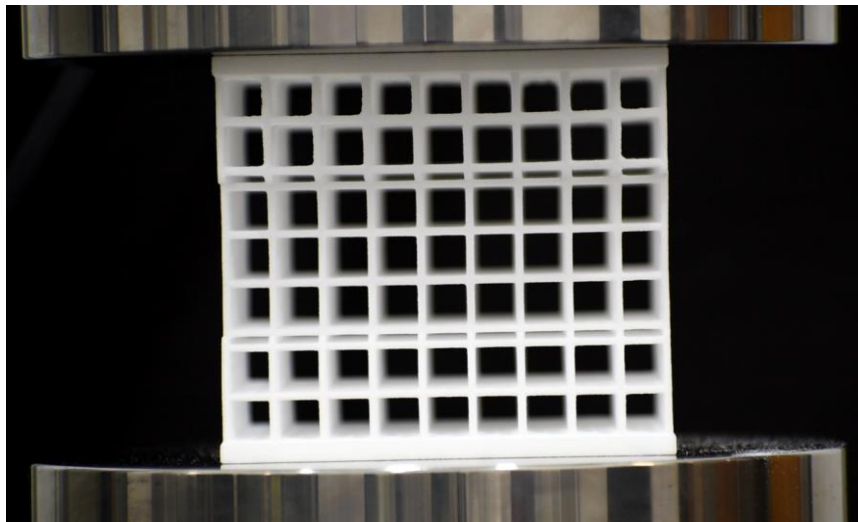


Figure 7- Example of a cube edge being subjected to compression loading

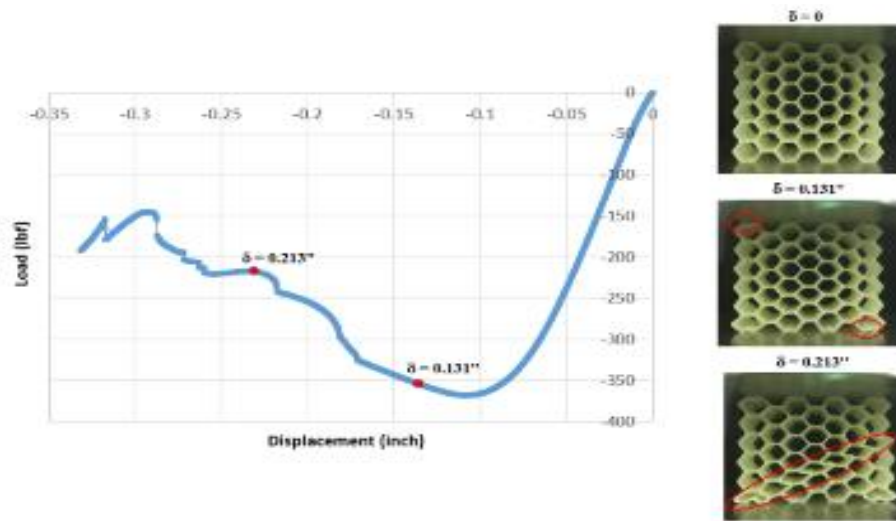


Figure 8- Properties of a hexagonal honeycomb being established for compression loading (Sharma et al. 2018)

A limitation of all the above approaches is that they are not extendable to three-dimensional structures, for which a design ecosystem that can relate local optimization of lattice shapes, sizes and parameters to global loads is needed.

Computational Tools for Lattice Design Optimization

The previous descriptions of lattice shape selection were based on analytical or empirical approaches that are attempting to extract unit cell behavior. As discussed before, this approach excludes structural realities in three-dimensional parts such as edge effects and neighbor-to-neighbor interactions, and is also limiting in its use for design optimization.

There are several computational tools and software available commercially to generate, optimize and evaluate the behavior of lattices, and create STL files for subsequent additive manufacturing. These capabilities have only been recently made commercially available, most being released within the last 3 years of writing this thesis. These software packages can be broken down into the following categories, as shown in Figure 9:

- Infill: These software tools generate a lattice within a solid design space with user-specified cell shape, size and thickness. The thickness and size of cells may vary across the structure, typically specified as a gradient. These lattices may later be imported to FEA solvers such as ANSYS or ABAQUS for analyzing their behavior under desired loading conditions. Examples include Simpleware, ANSYS SpaceClaim, Intralattice etc (Synopsys Inc, 2019), (ADML Labs, 2019). The limitation of the infill approach is that the design is not simulation driven in

response to local conditions and therefore relies heavily on design input and iteration.

- Homogenization: In the homogenization method, a Representative Volume Element (RVE) is analyzed for its behavior and properties and these obtained properties are scaled to an entire design space or solid body. Since the analysis is carried out on a single unit cell, the analysis is less computationally expensive. Examples of the homogenization approach include ANSYS Material Designer (Medikonda Sandeep, 2018), Altair OptiStruct (Altair Engineering Inc., 2019) etc. Since homogenization approaches do not involve explicit representation of lattice geometry in the analysis, they rely on valid and accurate characterization data for the effective properties of the lattice under consideration. These are challenging to obtain and extend reliably to domains beyond those tested experimentally.
- Generative Design: Generative design is a term that has come to represent design that is driven by simulation, as opposed to by direct specification by the designer. Topology optimization is one such example, where the software makes determinations on material removal, to arrive at the improved design. In the case of lattice structures, for example, a parameter like thickness can be determined by the solver which thickens lattices in regions of high stress. Examples include ParaMatters, (Bogomolny, Michael, 2018), NetFabb (Autodesk Inc., 2019), Element etc. All these methods explicitly represent the lattice geometry and can be computationally expensive, or involve the use of simplifying approaches such as representing struts as idealized beam elements, to arrive at results rapidly.

Since the goal of this research was to make comparisons between different unit cells, nTopology's Element software was selected due to its ability to explicitly represent lattice geometries and enable static FEA solutions, and also because of its computational speed, which allowed for rapid iteration.

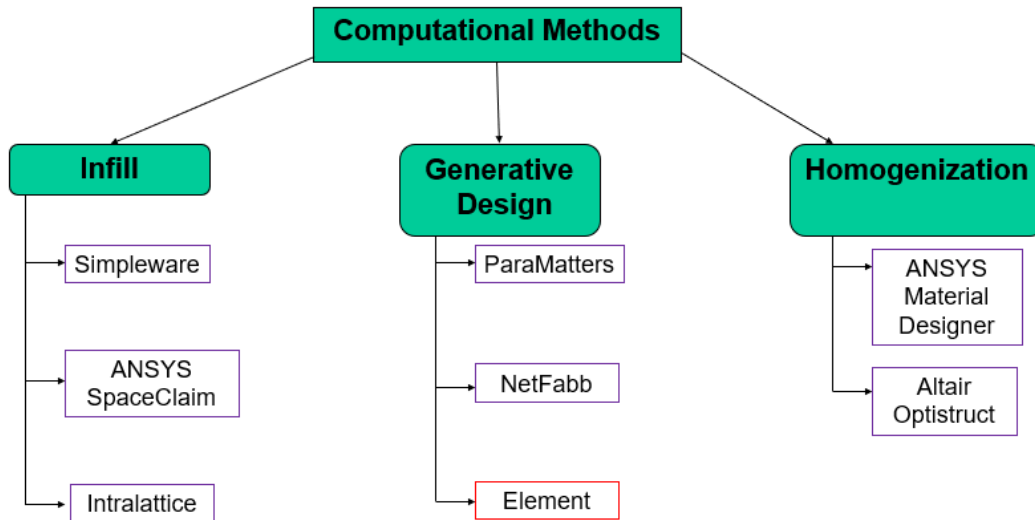


Figure 9- Commercial computational tools for lattice design optimization broadly fall into three categories

This thesis is divided into four main parts spanning the following three chapters. The next chapter deals with the computational and experimental methods used in the research work. The subsequent chapter provides details on the outcomes of these methods. The penultimate chapter interprets these results and identifies limitations of the current work. Finally, conclusions from this work are enumerated along with recommendations for future research.

METHODS

The main objective of this thesis is to compare responses of different lattice configurations under different loading conditions, but to do so at a structural, as opposed to a unit-cell level. In this chapter, the setups used for simulation across three test conditions: bending, tension and end-shear are described. Experimental methods used for compression testing are also discussed. At the outset, it is however important to define the metrics that were used to compare the different lattice shapes.

Response Metrics

This study examined the response of different lattice configurations to the applied loading conditions of bending, tension, and shear, at a given relative density. There was therefore a need to establish response metrics for each loading case, and to do so in a way that could isolate the effects of relative density and material composition from the overall response, to attempt a comparison on purely geometric accounts. These metrics are discussed for each loading condition of interest in this thesis.

Bending

For the case of symmetrical bending, we have the equation from classical mechanics:

$$\delta = \frac{PL^3}{48EI} \quad (8)$$

where, δ is the displacement or deflection developed in the middle of the beam of span L , which is made from a material with Young's modulus E , and has a Moment of Inertia I as a result of the applied load P (Hibbeler, 2004). In this equation, the product EI is

termed as flexural rigidity which is defined as the resistance offered by a structure while undergoing bending. Flexural rigidity is an ideal choice for a response metric as it relates resistance to bending of a structure to its displacement (δ) under a load for a given load L and span L . Displacement under loading is a simple parameter to determine in computational simulations as well as in experimental settings (such as a three-point bend test). The flexural rigidity of the lattice beam is normalized with the flexural rigidity of the solid beam of exact outer dimensions. This is done to discard the effect of the material selected for the lattice which gives the same or similar values when and if a different material is chosen for a similar analysis with the same lattice structure. The data for the PA 2200 material properties was obtained from the datasheet of the material provided by EOS (Electro Optical Systems, 2008). The flexural rigidity EI of a solid beam of PA 2200 material with the square cross-sectional area of 25x25mm is calculated as follows:

- Young's modulus (E) = 1700 MPa;
- Width of beam (b) = 25mm;
- Moment of Inertia (I) = $b^4/12 = (25^4)/12 \text{ mm}^4$
- Flexural Rigidity (EI) = 55.33 Nm²

So, the response indicator for the symmetrical bending load case is $(E^*I^*)/EI$ where (E^*I^*) is the bending rigidity of the lattice structure and EI is the bending rigidity of the solid beam with same outer dimensions as that of the lattice. This effective flexural rigidity is an indicator of how much the lattice structure will resist bending, the same way the flexural rigidity of a solid beam does.

A possible argument against the case of selecting the above metric is the fact that since cell shapes are being evaluated in this work of research and cell shape being a purely geometric property of the lattice structure, so evaluating simply the I^* , which can be described as the moment of inertia of the lattice beam, should be sufficient in analyzing the response of shape behavior under loading. But since the moment of inertia I of a solid beam depends purely on the dimensions of the two-dimensional cross-sectional area and since cross-sections of lattices have empty spaces in them and for some lattices the cross-sections are three-dimensional in nature. Therefore, isolating an effective moment of inertia for a lattice beam becomes a highly complicated task.

Tension

From classical mechanics we have the definition equation of Young's modulus which is formulated as

$$E = \frac{\sigma}{\varepsilon} \quad \dots(9)$$

where E is the Young's modulus of the material, σ is the normal stress developed during tensile loading for a normal strain ε (Hibbeler, 2004). Applied stress σ relates to applied force F and cross-sectional area A as

$$\sigma = \frac{F}{A} \quad \dots(10)$$

where F is selected arbitrarily, and A is also known and ε can be determined easily during simulation and experimentation. This allows the determination of E^* , which is defined as the effective Young's modulus of the lattice material under tensile loading. This effective

modulus is an indicator of how much the lattice structure will resist tension, the same way the tensile Young's modulus of a solid beam does.

The effective Young's modulus of the lattice beam is normalized with the Young's modulus of the solid beam of exact outer dimensions. This is done to discard the effect of the material selected for the lattice which gives the same or similar values when and if a different material is chosen for a similar analysis with the same lattice structure. The material chosen for all the lattices in this study is PA 2200 whose Young's Modulus (E) is 1700 MPa.

Hence, the response indicator for the tensile load case is E^* / E where E^* is the effective Young's modulus of the lattice structure and E is the Young's Modulus of the material from which the lattice has been manufactured from.

Torsion

From classical mechanics, for a square beam under bending, we have the equation,

$$\phi = 7.10 \frac{TL}{a^4 G} \quad \dots(11)$$

where ϕ is the angle of twist developed in a square beam of span L and side a subjected to a torque T whose made from the material with shear modulus G (Hibbeler, 2004). The simulation and experimental setup are the same as the conventional procedure for determining the shear modulus of a material where one end of the beam is fixed and the other end is subjected to torque T . Torque T is applied in the form of a force-couple who are related as

$$T = Fd \quad \dots(12)$$

where F is the value of shear force applied at opposite ends and d is the moment arm. Angle of twist ϕ is determined by the formula

$$\phi = \tan^{-1} \frac{\delta}{\left(\frac{a}{2}\right)} \quad \dots(13)$$

where δ is the planar lateral deflection due to twisting and a is the dimension of the side of the square beam.

Knowing the value of T , L and a , the shear modulus G becomes a function of lateral deflection δ . With this it is possible to determine G^* which is defined as the effective shear modulus of a given lattice structure. This effective modulus is an indicator of how much the lattice structure will resist twisting.

The effective shear modulus of the lattice beam is normalized with the shear modulus of the solid beam of exact outer dimensions. This is done to discard the effect of the material selected for the lattice which gives the same or similar values when and if a different material is chosen for a similar analysis with the same lattice structure. The material chosen for all the lattices in this study is PA 2200 whose shear modulus (G) is 609.7 MPa (Electro Optical Systems, 2008).

Hence, the response indicator for the tensile load case is G^*/G where G^* is the effective Young's Modulus of the lattice structure and E is the Young's Modulus of the material from which the lattice has been manufactured from.

Simulation Setup

The lattice generation and analysis were performed using ‘Element’ which is a generative design software tool developed by nTopology Inc., a New York based startup that launched in 2012. Element has several useful features for the designer of lattices, but for the purposes of this work, the tool can be broken down into two parts:

Lattice Generation - First, a CAD file of the beam of dimensions 25mm x 25mm x 25mm (design space) is imported into the software and populated with the required cell shape. The cell shape is chosen by the user from the library of shapes available under the ‘Rule’ category, as shown in Fig. 10. The design space can be filled with the chosen cell shapes in three ways, namely ‘Centroid’, ‘Fill-Inside’ and ‘Fill Completely’. Number of cells in each direction of the beam is controlled by the rule scale. The Fill Type and Rule scale are chosen in such a way for each shape that they fit into the design space as closely as possible for a chosen shape. Once the parameters have been decided for the lattice, the software then generates a lattice as shown in Fig. 11.

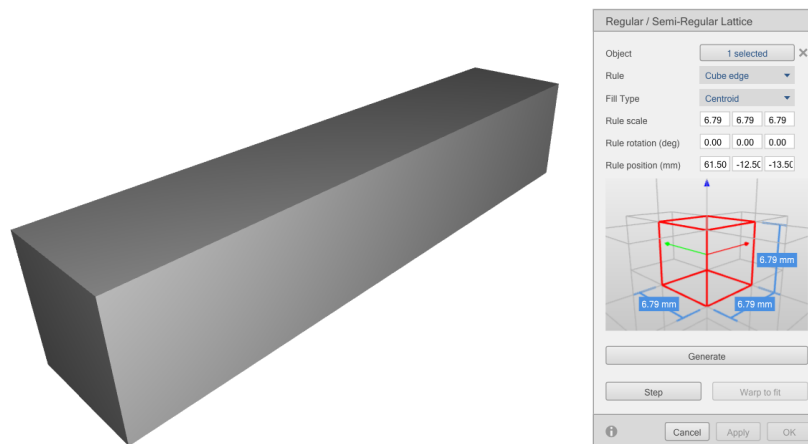


Figure 7- Imported geometry with chosen lattice shape and rule

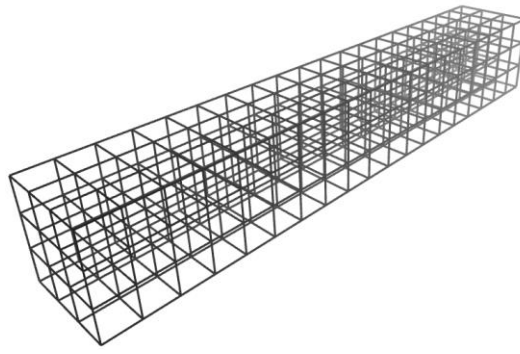


Figure 8- Lattice Tessellation of Imported Geometry

For this work of research, 13 periodic unit cell lattices and stochastic lattices were chosen for analysis arbitrarily. The different shapes are shown in the flow-chart in Fig. 12. The 13 shapes can be classified in terms of tessellation, as cube, hexagonal prism and tetrahedron.

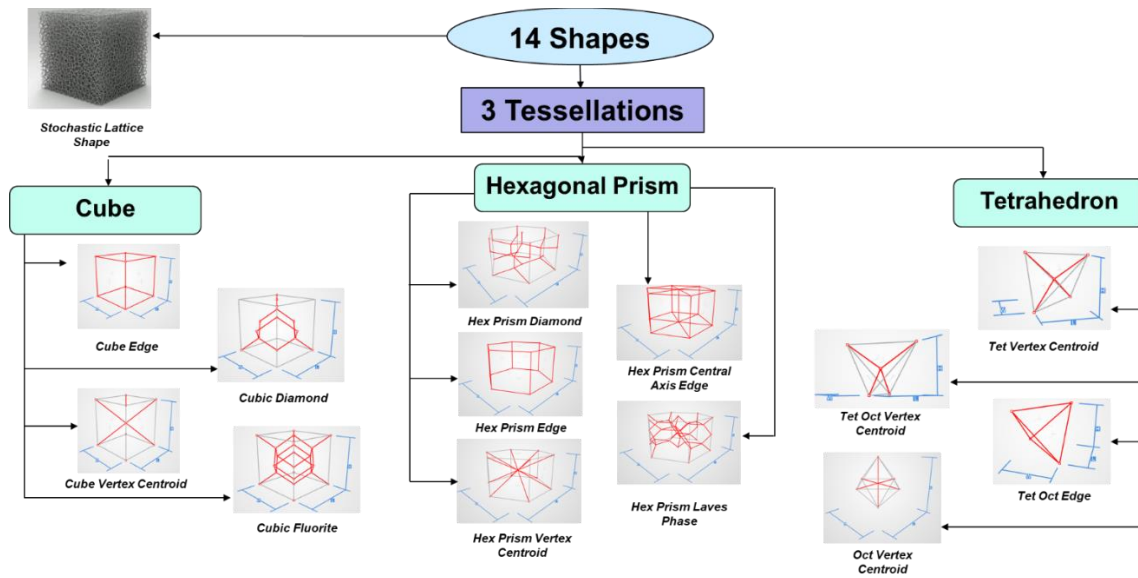


Figure 9- Classification of chosen cell shapes on basis of tessellation

Simulation – The software takes into consideration the effects of only small deformations i.e. performs only linear analysis. Once the lattice has been generated, it can now be imported into the ‘Analysis’ environment. In this environment, boundary

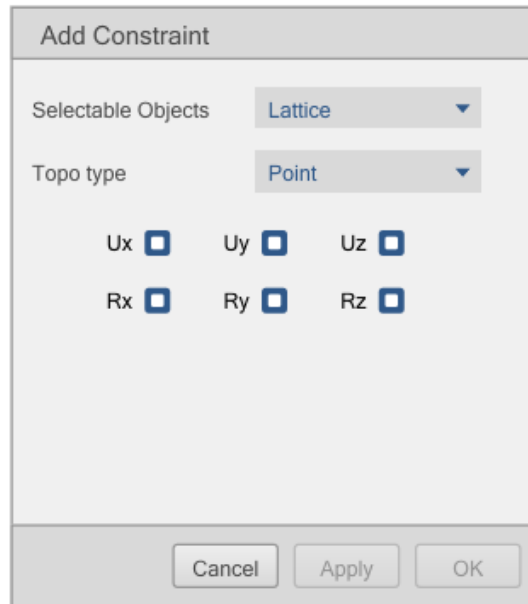
conditions and loads can be imposed on the lattice, which will thicken the lattice according to the Stress Minimization algorithm of the software. This algorithm decreases or increases the thickness of the struts in order to minimize the stress so that it is in the permissible range of the specified maximum stress. The analysis environment can also conducted stress analysis without any optimization required.

Element allows you to import selection objects, as shown in Fig. 13, which is the design solid and a plane at the middle of the design space solid in this case. The purpose of selection solids is to provide an edge, surface or point to the design space directly rather than the individual nodes of the lattice, which can be time-consuming if done manually.




Figure 10- Selection objects in Element analysis tool

Constraints can be applied to both lattices as well as the selection objects, as shown in Fig. 14. The 'Add Constraint' allows the user to restrict or free the six degrees of freedom (three translational and three rotational). The Add Load toolbox shown in Fig. 15 allows to apply forces in the x,y and z directions. These can be applied directly to lattice structures or selection objects, as shown in Fig. 16.



The 'Add Constraint' dialog box features a title bar at the top. Below it, there are two dropdown menus: 'Selectable Objects' set to 'Lattice' and 'Topo type' set to 'Point'. In the center, there are six checkboxes arranged in two rows of three, labeled Ux, Uy, Uz in the top row and Rx, Ry, Rz in the bottom row. All checkboxes are currently unchecked. At the bottom of the dialog, there are three buttons: 'Cancel', 'Apply', and 'OK'.

Figure 11- Constraints for structural loading applications



The 'Add Load' dialog box has a title bar. Below the title bar, there are two dropdown menus: 'Selectable Objects' set to 'Lattice' and 'Load type' set to 'Point load'. Underneath these are three input fields for force components, labeled Fx (N), Fy (N), and Fz (N). Each field contains the value '0.0'. At the bottom of the dialog, there are three buttons: 'Cancel', 'Apply', and 'OK'.

Figure 12- Add load toolbox

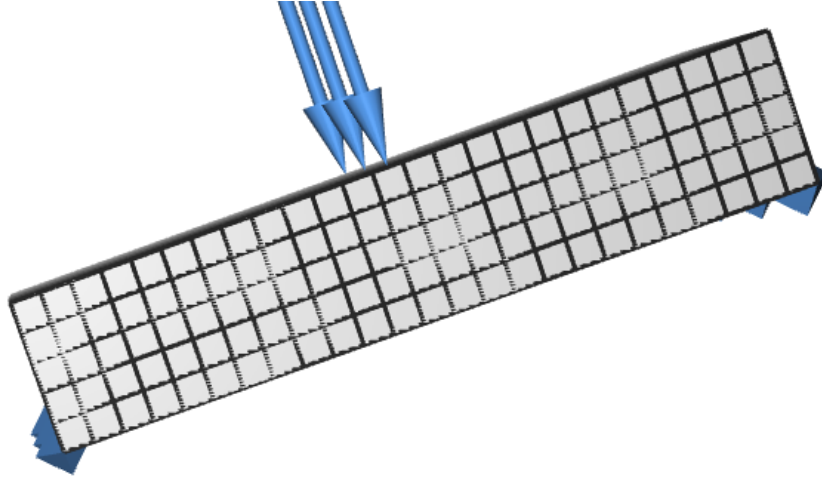


Figure 13- Application of boundary conditions and forces for symmetric bending case

After the application of constraints and boundary conditions, the software gives the solution. The solution can be solved for minimizing stress or minimizing strain. All the solutions in this study are generated for the minimization of stress case.

As can be seen from the Fig. 17, the analysis setup requires one to specify if the optimization is for stress or strain as discussed earlier, with the aim of keeping the design solution under that value. For this study, the maximum allowable stress was set to several times the true material yield stress value. This was done in order to obtain a value of stress and displacement to complete the observation plots, independent of nonlinear response of the base composition itself. The two material properties required by the software were Young's modulus and Shear modulus. The Young's modulus of the chosen material, PA 2200, is 1700 MPa and the shear modulus of the same is 609.7 MPa. After this the parameter needed to be defined was the maximum and minimum node thickness of the lattice. The user has the full freedom to keep this constraint free and allow the

solver to decide the thicknesses of all the struts across the lattice. In this study however, in order to vary the relative density for lattice of each shape, uniform thickening was done. In order to do that the node thicknesses were locked down, and a lattice of a specific node thickness was generated.

Solve - Beam Size Optimization

Optimization Objective

Optimize for

Stress

Max stress (MPa)

9800

Material Properties

Young's modulus (MPa)

1700

Shear modulus (MPa)

609.7

Optimization Parameters

Iterations

25

Min diameter (mm)

☒

1.8

Max diameter (mm)

☒

1.8

Center of Mass Optimization

Optimize CoM location

☐

Desired CoM

0.000

0.000

0.000

Smoothing steps

1

Allowed CoM tol.

☐

0.05

Mesh resolution

☐

0.05

Cancel

Solve

Figure 14- Element analysis solution setup

Finally, the solution is generated, and contour plots of stresses and displacements can be seen as shown in Fig. 18, and volume associated with that structure and its

bounding box can then be estimated as shown in Fig. 19. Relative Density (ρ^*/ρ) is defined as the density of the lattice divided by the density of the bounding solid. In this entire study, for every lattice of every shape, the value of the metric corresponding to each shape, has been determined over the range of 0.01 to 0.3 relative density. This relative density range has been chosen as Gibson & Ashby define this range as the range for lattices, and from 0.3 to 0.5 to that of foams (Gibson & Ashby, Cellular Solids by Lorna J. Gibson, 1997).

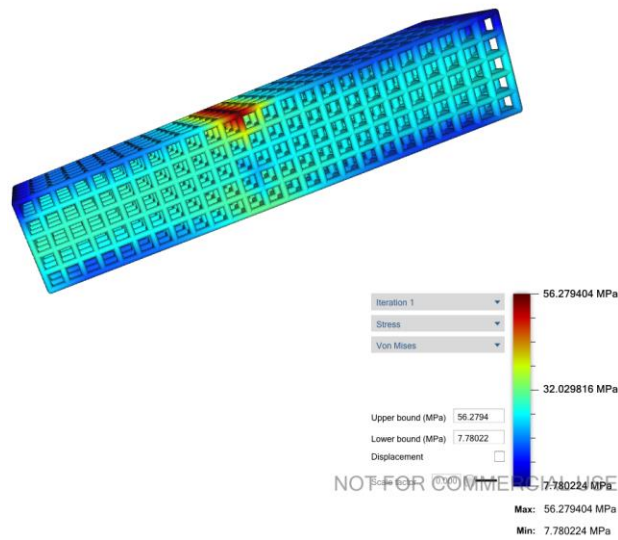


Figure 15- Sample solution of symmetric bending problem

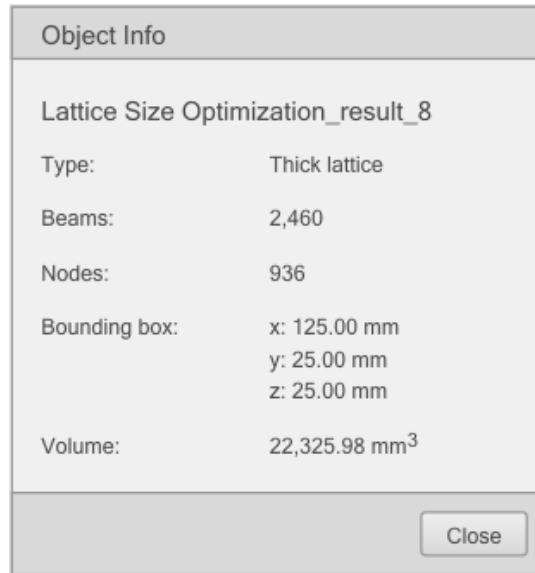


Figure 16- Object info result to calculate volume of thickened lattice

Stochastic Lattices

The first step in generating a stochastic lattice is selecting the design space imported in the software, following which the rule is selected. For the entire study in this work, Voronoi is chosen as the 'Rule'. Then the target cell diameter is chosen. Target cell diameter is defined as the average cell diameter of the stochastic lattice. For the entirety of this study, the target cell diameter is 5mm. The final parameter to be chosen is the 'Random Seed'. Random seed is an input to the in-built random seed generator function. The mechanism of seed generators is explained as follows.

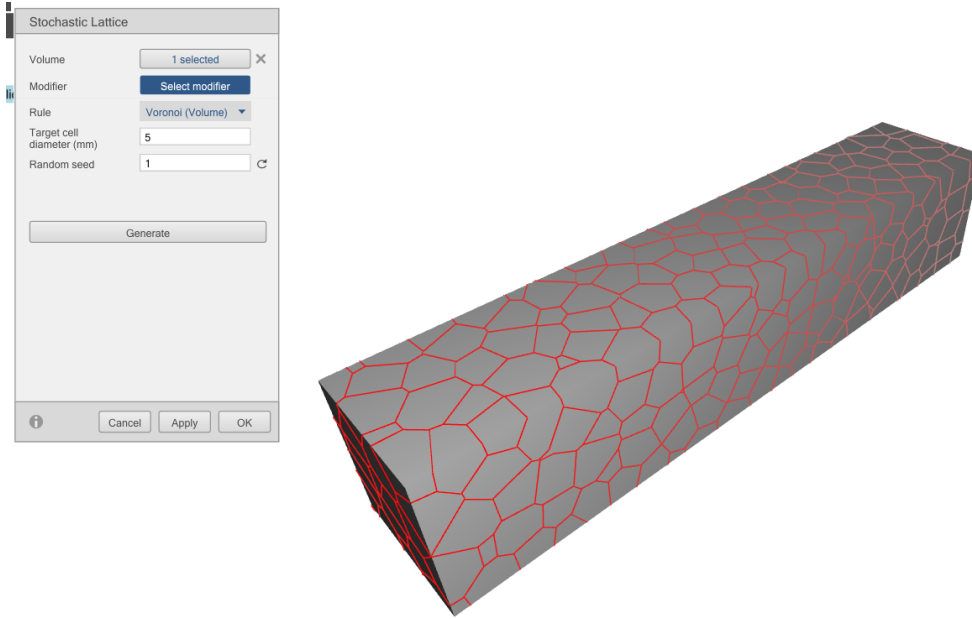


Figure 17- Stochastic lattice generation

The randomness of the stochastic distribution is implemented using pseudorandom number generators (PRNGs). The sequence of random number that are generated are not truly random. They are pseudorandom, as they start to repeat after some time. For example, one of the PRNGs, the Mersenne Twister has a very long period of $2^{19937}-1$ numbers (Eindhoven University of Technology, 2019)

Since the sequence of numbers generated is always the same, the only way to vary it, is to use a different starting place. The starting place is determined by the ‘Random Seed’ value that we choose. This is one of the key features of Element when it comes to stochastic shapes, a certain value of a random seed will always correspond to the same Voronoi configuration allowing to evaluate the same stochastic configuration repeatedly

under different loading cases. Stochastic configurations in the entire text are designated as *Stochastic Seed- “Random Seed Value Assigned”*.

Simulation for Beam Bending Case

The first step was importing the geometry in Element and assigning the suitable cell shape and rule that just fits the design space beam of 25x25x125mm. Then that generated lattice is imported to the analysis environment for thickening. A load of 300 N in the downward direction is applied with the degrees of freedom $U_x=R_x=R_y=0$. The displacements in the y and z direction and rotations in x have been kept free so as to simulate the effect of rollers which would exist in a three-point bend test, the standard procedure to determine bending rigidity of beams.

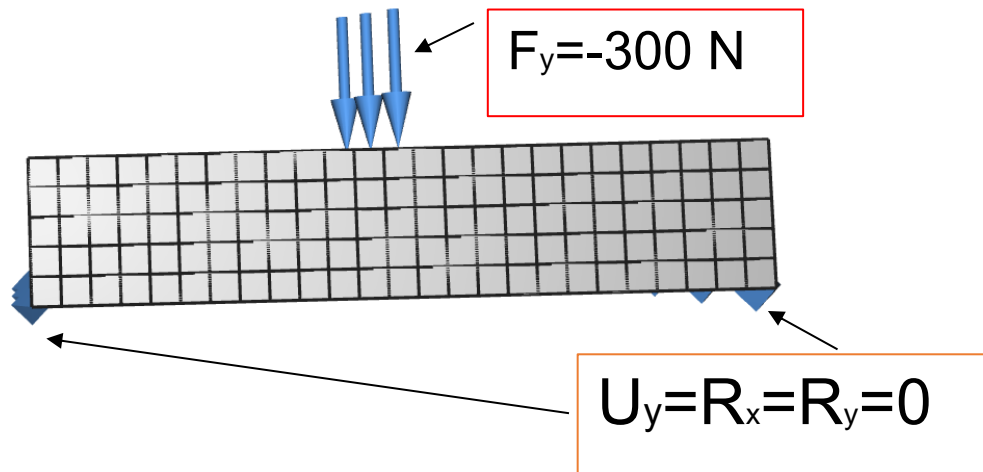


Figure 18- Symmetric bending load case with applied load and constraints

Then the lattice is thickened for a fixed node thickness whose volume can now be determined from Object Info. The displacement in the y-direction are noted and from that

the Relative Bending Rigidity (E^*I^*/EI) is calculated for a given relative density as discussed in the derivation of metrics section.

Simulation for Tensile Loading Case

The first step was importing the geometry in Element and assigning the suitable cell shape and rule that just fits the design space beam of 25x25x125mm. Then that generated lattice is imported to the analysis environment for thickening. A load of 50N each is applied on the four edges on one of the faces on the axial direction, whose net sum of forces comes out to be 200N in the axial direction. The other end of the beam is constrained fully except the translational degrees of freedom in the transverse (U_y and U_z , if force is applied in x-direction). The reason is to allow for lateral deformation while the beam is under bending.

Then the lattice is thickened for a fixed node thickness whose volume can now be determined from Object Info. The displacement in the x-direction is noted and from that the Relative Young's Modulus (E^*/E) is calculated for a given relative density as discussed in the derivation of metrics section.

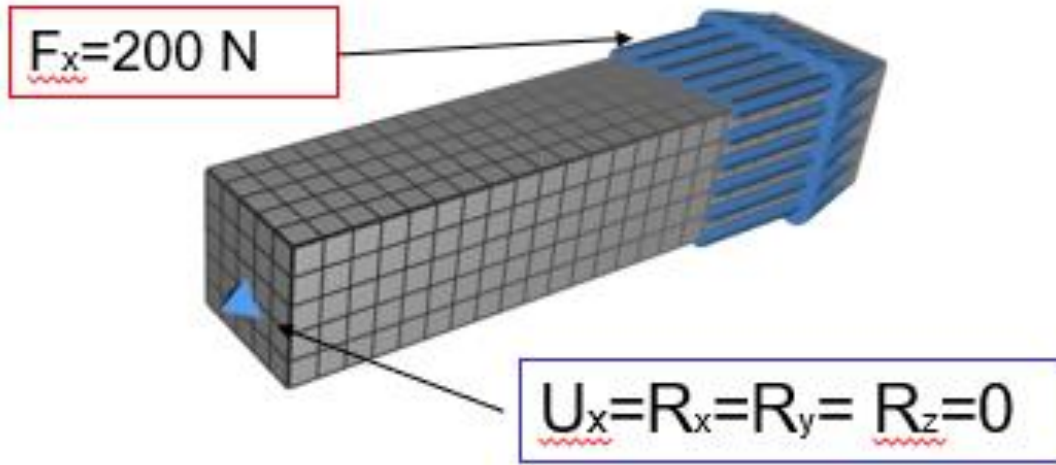


Figure 19- Tension load-case with applied load and constraints

Simulation of Torsional Case

The first step was importing the geometry in Element and assigning the suitable cell shape and rule that just fits the design space beam of 25x25x125mm. Then that generated lattice is imported to the analysis environment for thickening. Two equal and opposite forces of 50N are applied in the lateral direction (y direction) to generate a torque of $50\text{N} \times 25\text{mm} = 1250\text{Nmm}$. The opposite end of the beam is fully constrained.

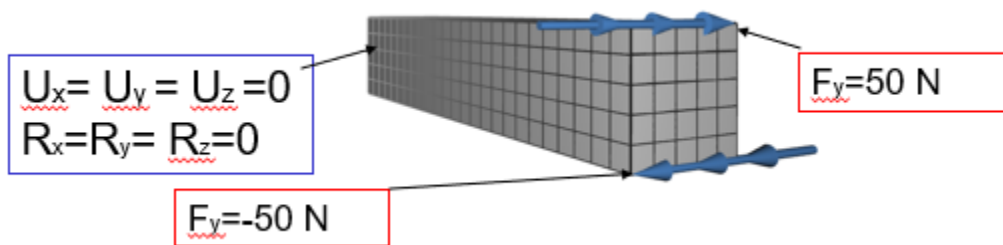


Figure 20- Torsion load case with applied load and constraint

In this way, the torsional test for shear loading conditions is performed for lattices so as to calculate the relative shear modulus of the lattice as a function of its relative displacement (as discussed earlier).

Then the lattice is thickened for a fixed node thickness whose volume can now be determined from Object Info. The displacement in the y-direction is noted and from that the Relative Shear Modulus (G^*/G) is calculated for a given relative density as discussed in the derivation of metrics section.

Manufacturing of Lattice Specimen for Experimental Tests

In order to determine how the simulation results obtained fare-up in real physical environment, mechanical compression testing was performed. For testing, each of the 13 periodic cell shape lattices and two stochastic lattices were chosen. These specimens were manufactured in the Manufacturing Hub at the ASU Polytechnic campus using the Selecting Laser Sintering (SLS) process.

While designing the lattices for each of the unit cells it was ensured that in each direction, there are a minimum 6-8 cells in each direction so as to extract stable values for mechanical characterization of lattice structures as demonstrated by Le (Le et al. 2017).

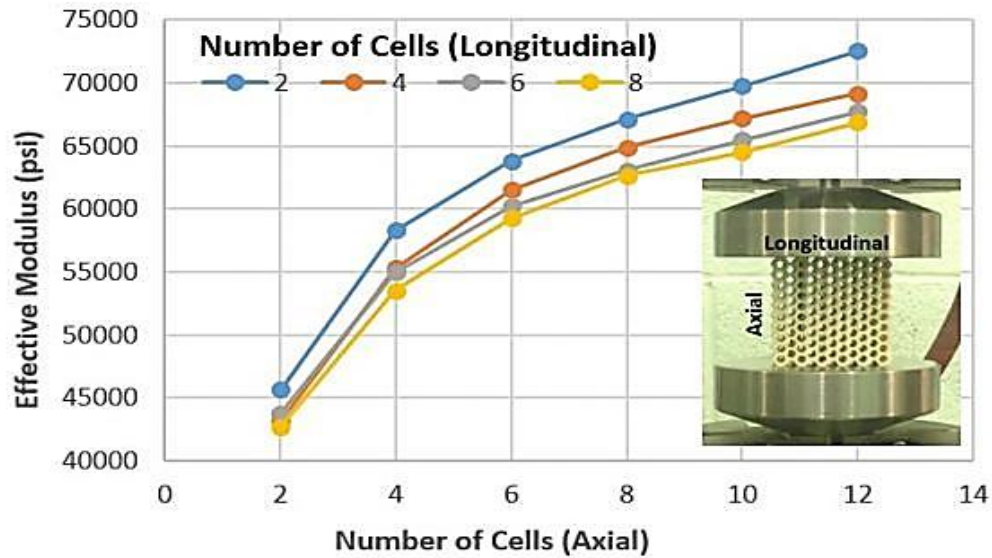


Figure 21- Effect of number of cells for determining mechanical properties (*Le et al. 2017*).

The first step was generating .STL files for each of the specimens. STL is the format recognized by SLS printers and all other kinds of additive manufacturing machines for printing. For generating these files, Element was used as Element allows you to convert thickened lattices to lattices using the ‘Import’ function in the software.

Each of the lattice files consisted of a design space of dimensions 80mm x 80mm x 80mm, which was lattice optimized for a corresponding shape. In order to assist in testing, two plates were also designed with the lattice, one at the top and one at the bottom with dimension, 82mm x 82mm x 3mm.

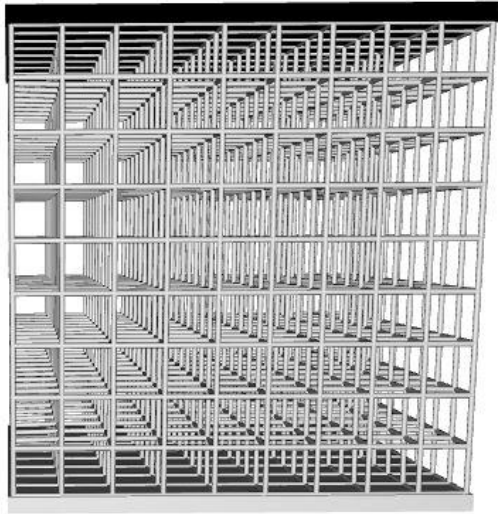


Figure 25 (a)

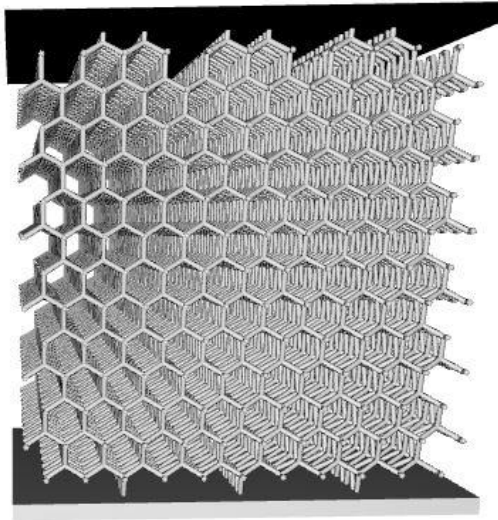


Figure 25(b)

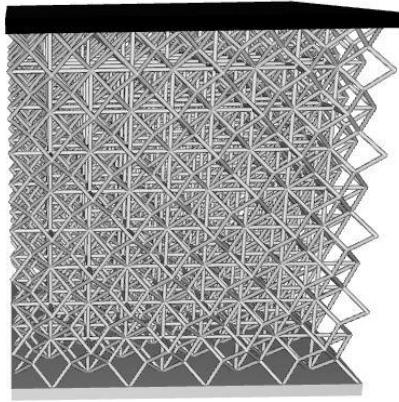


Figure 25(c)

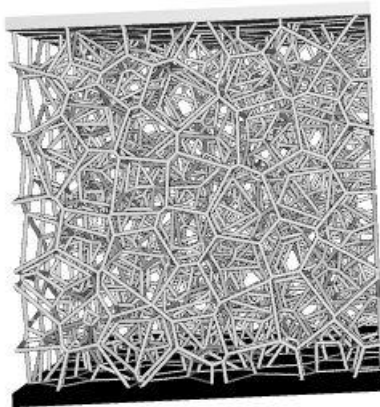


Figure 25(d)

Figure 22 (a),(b),(c),(d) – CAD files of testing specimen of Cube Edge, Hex Prism Vertex Centroid, Tet Oct Vertex Centroid and Stochastic Seed-61 respectively

Once converted to STL, these files are now imported to Magics software by Materialise for slicing the parts into layers for the printing process. For the printing or manufacturing process, ‘EOS Formiga P 110’ SLS printer was used. The SLS powder

process begins with a bin of the polymer powder being heated to a temperature just below the melting point of the polymer. A recoating blade deposits a very thin layer of the powdered material (typically 0.1mm) onto a build platform. A CO₂ laser beam then starts to scan the surface. This laser selectively sinters the powder and solidifies a cross-section of the part. The laser is focused to the correct location by a pair of galvanometers. When the entire cross section is scanned, the building platform moves down one layer in thickness height. The recoating blade deposits a new layer of powder on top of the recently scanned layer and the laser starts to sinter the successive cross section of the part onto the previously solidified cross-sections. This process is repeated until all parts are fully manufactured. Unsintered powder remains in place to support the part as it is built, eliminating the need for support structures. This is one of the major advantages of SLS. The result is a bin filled with powder and consolidated products. Since multiple products can be produced simultaneously, all the specimens were printed in two batches.

The orientation of the parts was the two plates and the lattice lying on the build-plate. Such an approach removes the requirement for support structures, hence reducing material and cost. Another alternative approach could have been one of the testing plates of the specimen lying flat on the build plate supporting the structure upright. But this approach was not adopted as that flat surface of large surface would have experienced large amounts of warping due to thermal gradients that get set-up, hence affecting the quality of the part. After the printing process and the powder bin and parts have down, the powder bin is unpacked. The printed parts were then parted from the unsintered powder and cleaned with compressed air and brushes.

Compression Testing of Specimens

Compression testing was carried out on Instron 8801 servohydraulic mechanical tester. All 15 specimens were made to undergo quasi-static compression testing. The tester had 50kN load cell and was armed at 48kN to avoid any damage to the load cell which means the test would stop just as the force generated would reach 48kN. A spherical seat setup was placed on the top of the compression plate which was restricted in the beginning when the top and the bottom plate are matched. This was done so as to match the parallelism between the top and bottom plate and avoid measurement errors.

The inbuilt software collects data in the form of force-displacement graphs. The entire experiment is divided into cycles. Time defined for one cycle is 240 seconds and the data acquisition was made at 250 data points per cycle. Hence, one data point is generated after every 0.96 seconds. This is carried out till the compression comes to an end or the load exceeds the safe load value.

The specimens were placed upright on the machine prior to testing and compression videos were captured during testing. The length of travel was set to be 80mm (which is the length of the specimen excluding the width of the build plate). The strain rate for the experiment is set to be 10^{-3} /second for each of the specimens.



Figure 23 - Instron 8801 Servohydraulic Mechanical Tester at the ASU Polytechnic campus that was used in this work

RESULTS

This chapter presents the observations and results of the simulations and testing carried out as per the methods discussed in the previous section.

Bending Load Case

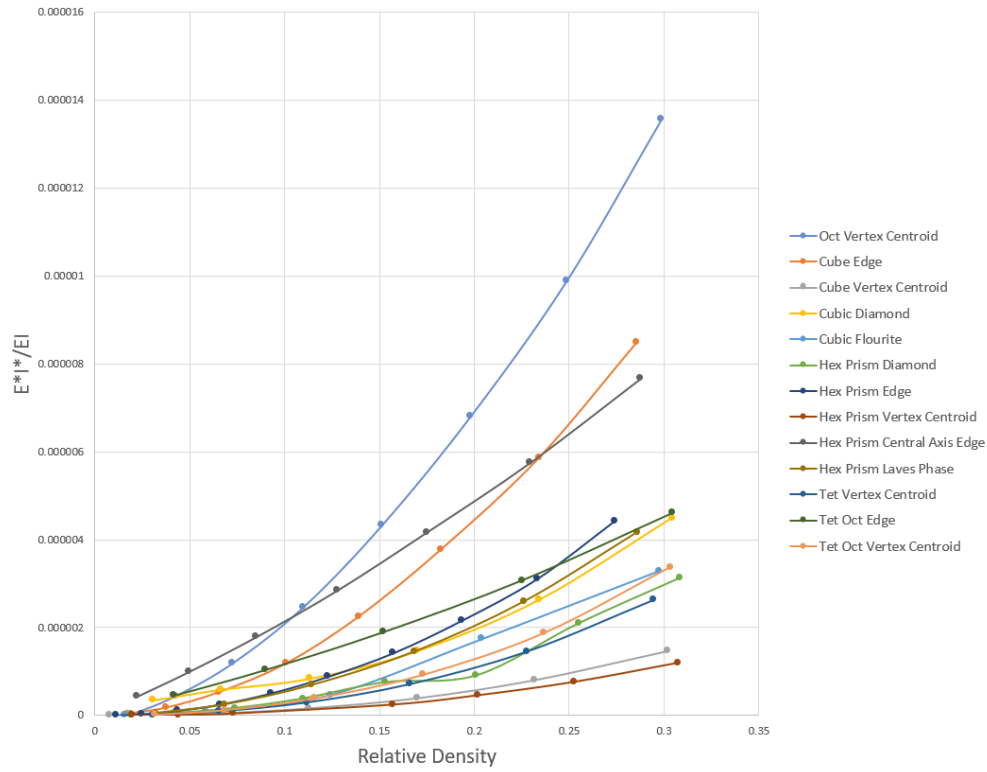


Figure 24- Relative bending rigidity versus relative density plot for periodic shapes

The graph shown above was generated for all the periodic shapes over a range of relative density for the relative bending rigidity (E^*I^*/EI). This plot shows that Oct Vertex Centroid has the highest value of relative bending rigidity over the lattice range of relative density of all the regular periodic shape lattices. The range of relative density is developed by varying the node thicknesses of the lattices in each case.

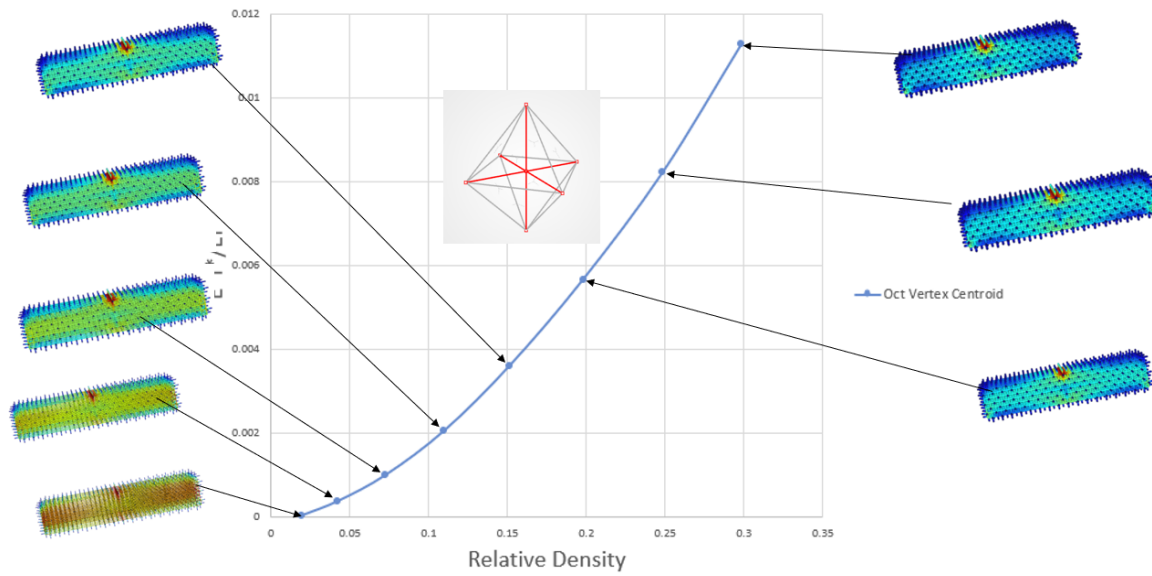


Figure 25- Relative bending rigidity versus relative density plot and corresponding contour plots for Oct Vertex Centroid

The above plot shows the relative bending rigidity of Oct Vertex Centroid over the range of lattice relative density. This plot also shows the stress contour plots for Oct Vertex Centroid at different intervals of relative density. It can be seen that as the thickness and through that the relative density increases, the stress bearing capacity of the lattice also increases.

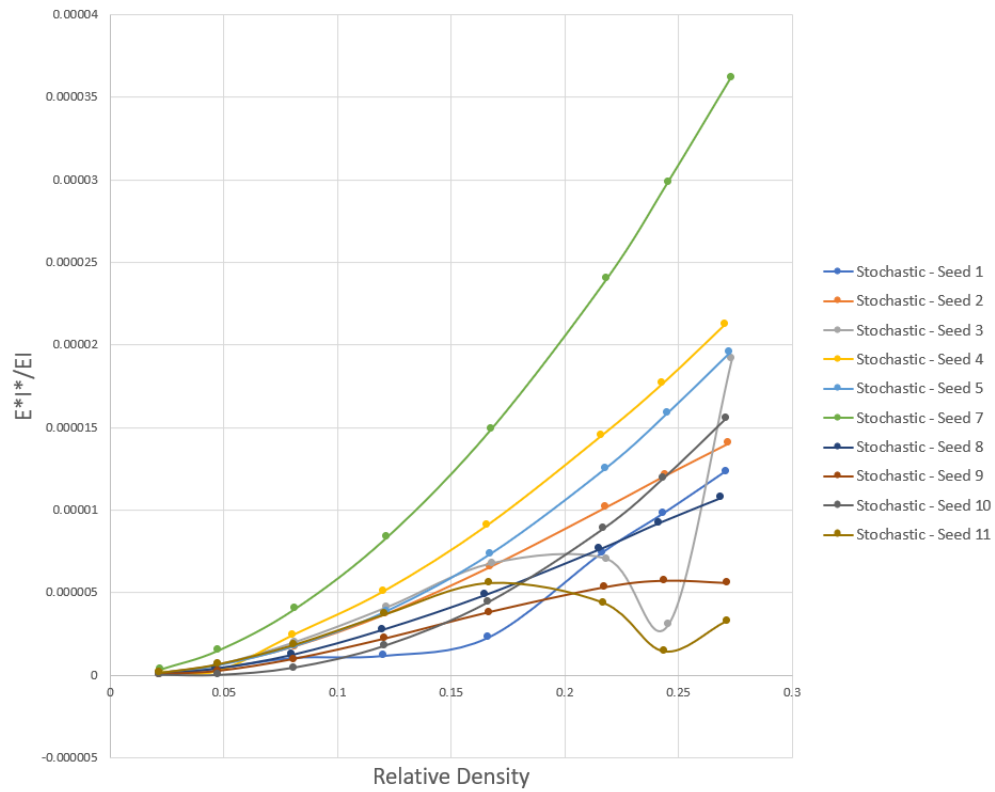


Figure 26- Relative bending rigidity versus relative density plot for stochastic shapes

Next, the response of stochastic structures to bending load was analyzed. For this, stochastic structures with different seed values from 1 to 11 were taken. These seed values were found to be ample for a complete analysis of the stochastic shapes under symmetric bending.

When each of these shapes were plotted for their metric values versus the corresponding relative density, over the lattice density range, the plot shown above is observed. It can be seen that over the selected range of relative density, Stochastic-Seed7 has the highest value of relative bending rigidity.

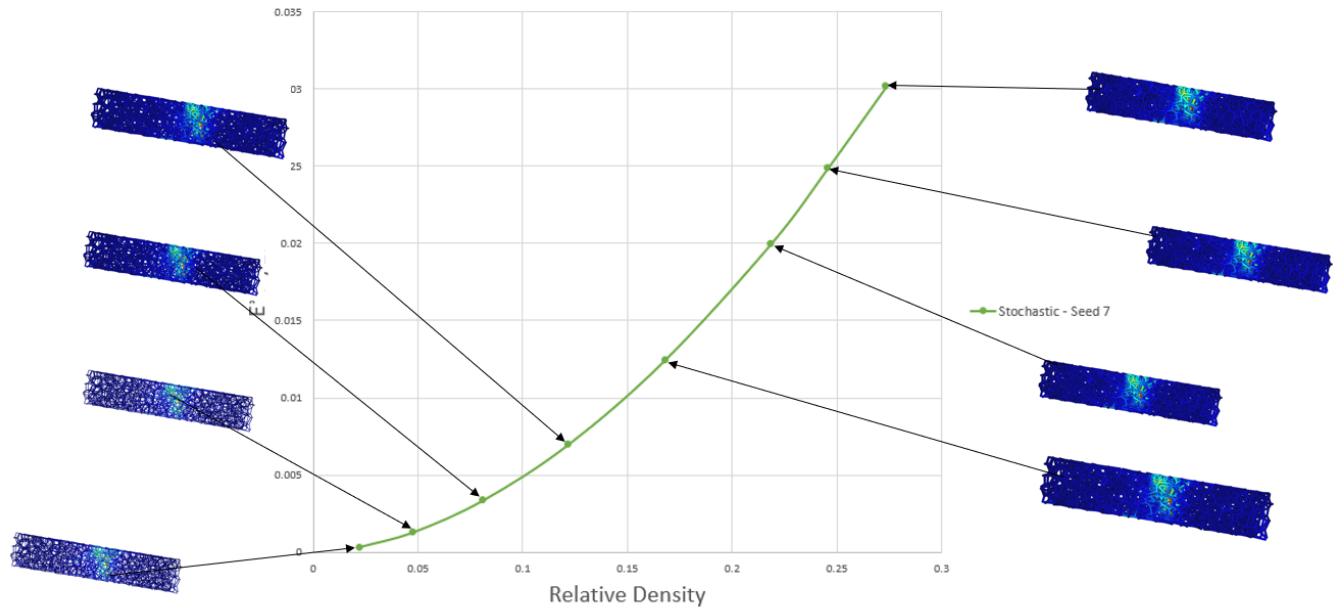


Figure 27- Relative bending rigidity versus relative density plot and corresponding contour plots for Stochastic- Seed 7

The above plot shows the relative bending rigidity of Stochastic-Seed 7 over the range of lattice relative density. This plot also shows the stress contour plots for Stochastic-Seed 7 at different intervals of relative density. It can be seen that as the thickness and through that the relative density increases, the stress bearing capacity of the lattice also increases and the stress is more or less concentrated in the middle of the lattice.

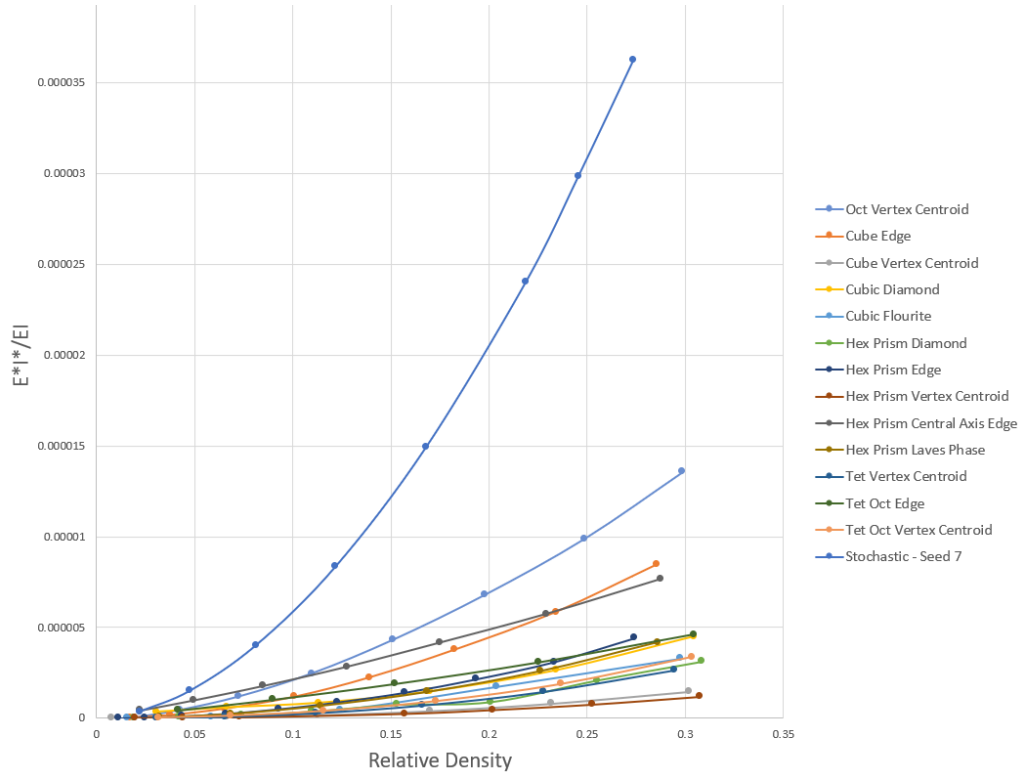


Figure 28- Relative bending rigidity versus relative density plot for Stochastic-Seed 7 and periodic shapes

Stochastic Seed-7, the stochastic shape with the highest value of relative bending rigidity was plotted along with the other periodic shape. As can be seen from the plot above, Stochastic Seed-7 has the highest value of relative bending rigidity when compared to all the periodic shapes over the entire range of lattice relative density. This points to the fact that for the symmetrical bending load case, stochastic structures have the potential to surpass periodic cell shapes in terms of resistance to bending load.

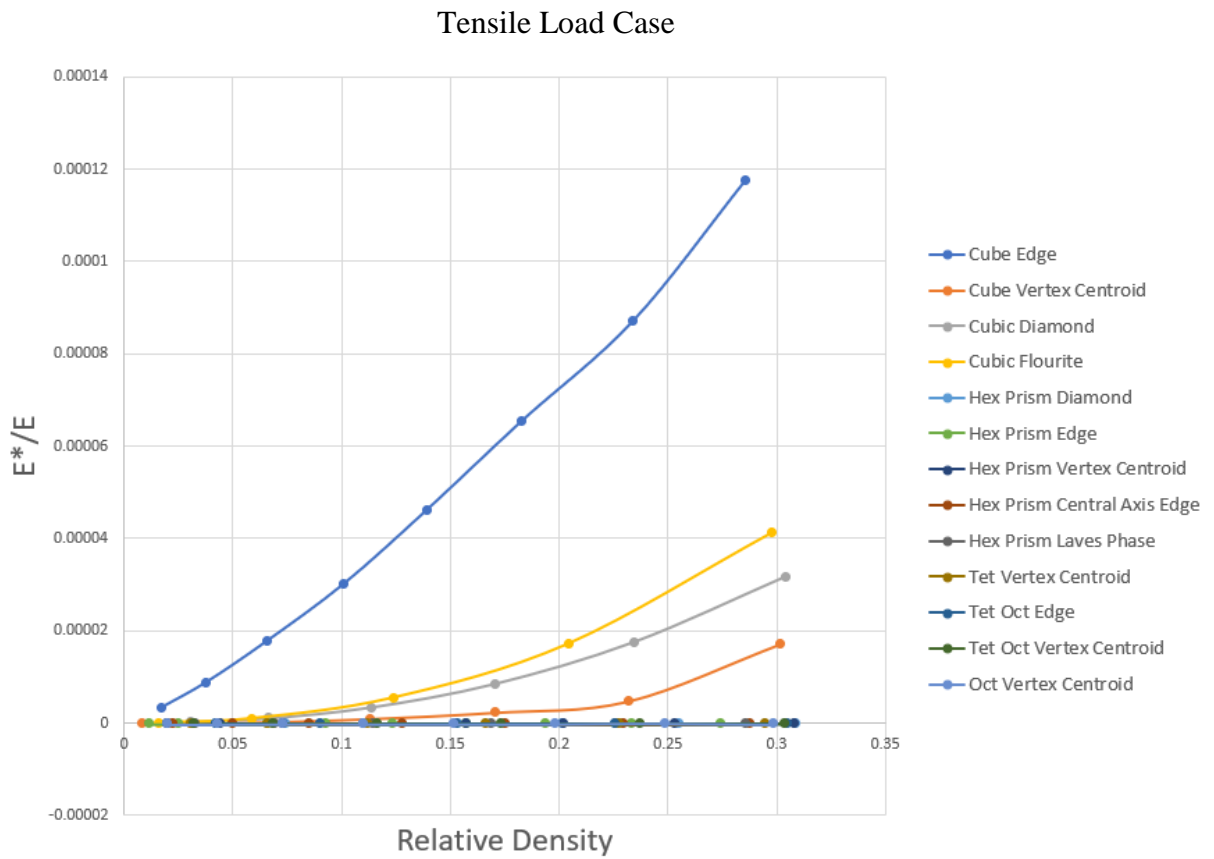


Figure 29- Relative Young's modulus versus relative density plot for periodic shapes

The graph shown above was generated for all the periodic shapes over a range of relative density for the relative Young's modulus (E^*/E). This plot shows that Cube Edge has the highest value of relative Young's modulus over the lattice range of relative density of all the regular periodic shape lattices. The range of relative density is developed by varying the node thicknesses of the lattices in each case.

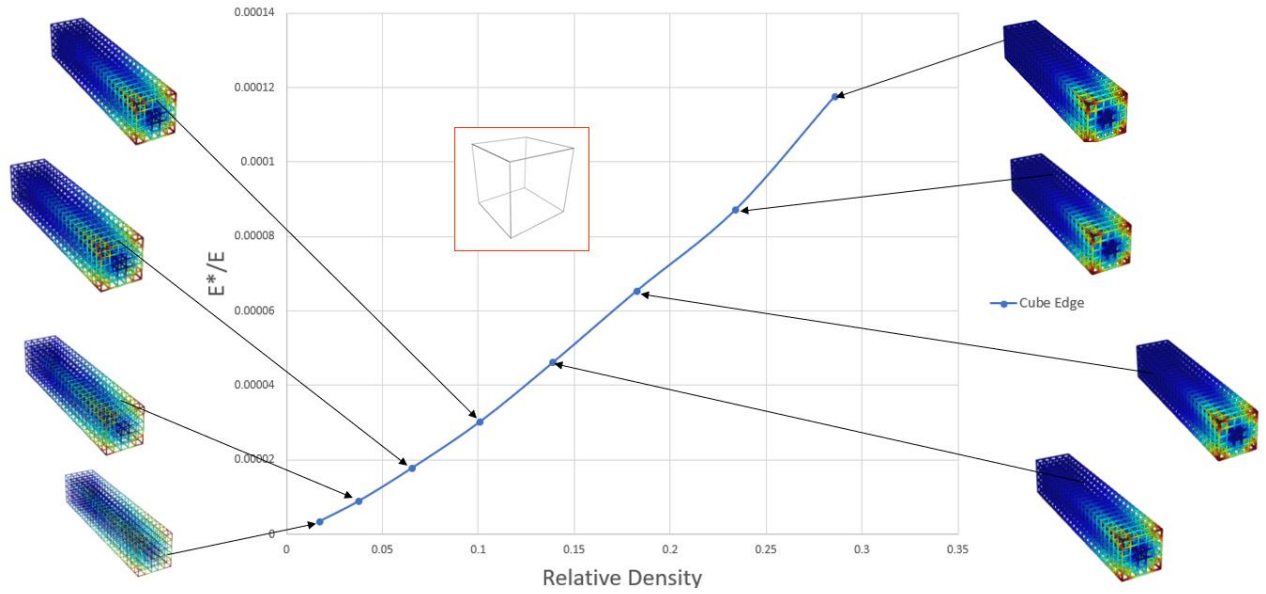


Figure 30- Relative Young's modulus versus relative density plot and corresponding plots for Cube Edge

The above plot shows the relative Young's modulus of Cube Edge over the range of lattice relative density. This plot also shows the stress contour plots for Cube Edge at different intervals of relative density. It can be seen that as the thickness and through that the relative density increases, the stress bearing capacity of the lattice also increases.

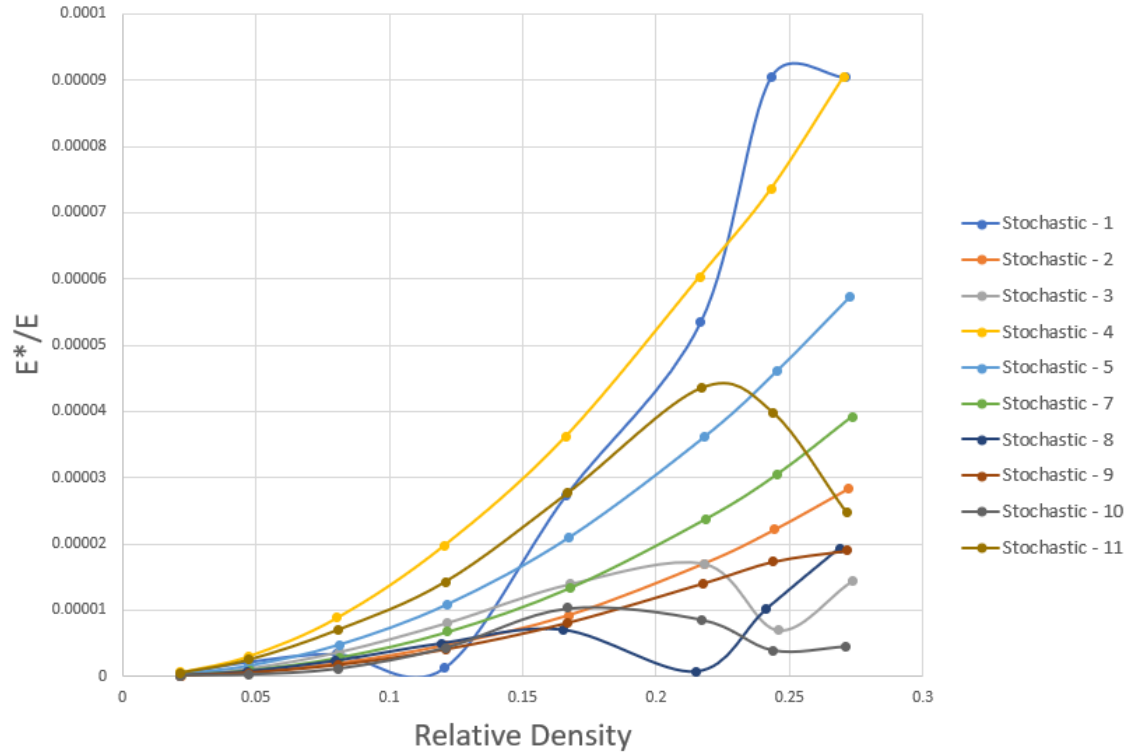


Figure 31- Relative Young's modulus versus relative density plot for stochastic shapes

Next, the response of stochastic structures to tensile load was analyzed. For this, stochastic structures with different seed values from 1 to 11 were taken. These seed values were found to be ample for a complete analysis of the stochastic shapes under tensile loading. When each of these shapes were plotted for their metric values versus the corresponding relative density, over the lattice density range, the plot shown above is observed. It can be seen that over the selected range of relative density, Stochastic-Seed4 has the highest value of relative Young's modulus.

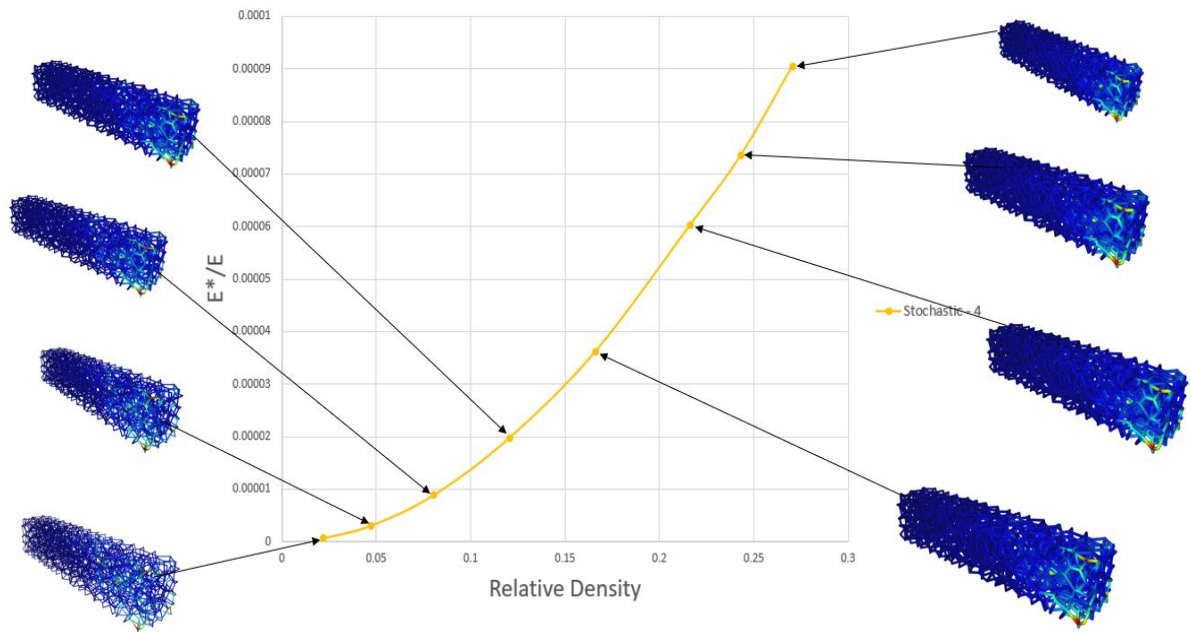


Figure 32- Relative Young's modulus versus relative density plot and corresponding contour plots for Stochastic- Seed 4

The above plot shows the relative Young's modulus of Stochastic-Seed 4 over the range of lattice relative density. This plot also shows the stress contour plots for Stochastic-Seed 4 at different intervals of relative density. It can be seen that as the thickness and through that the relative density increases, the stress bearing capacity of the lattice also increases.

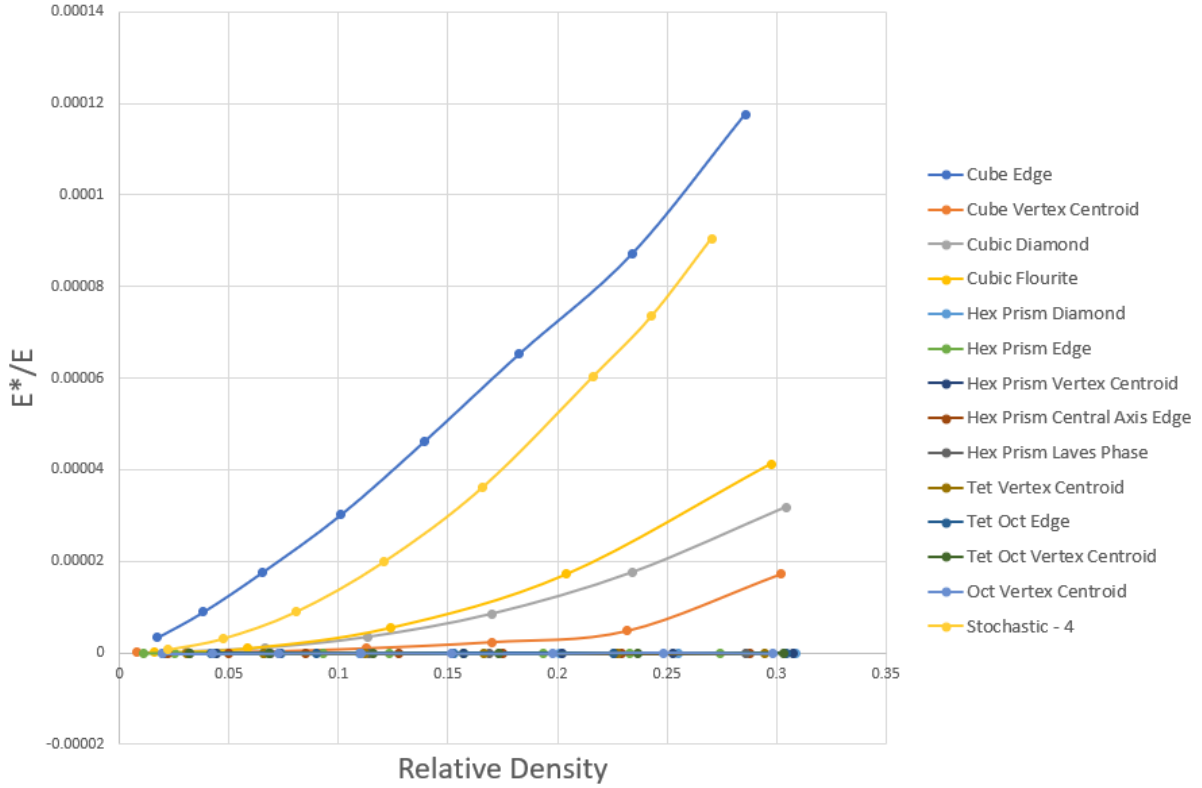


Figure 33- Relative Young's modulus versus relative density plot and corresponding contour plots for Stochastic- Seed 7 and periodic shapes

Stochastic Seed-4, the stochastic shape with the highest value of relative Young's modulus was plotted along with the other periodic shapes. As can be seen from the plot above, Stochastic Seed-4 has the second highest value of relative bending rigidity when compared to all the periodic shapes over the entire range of lattice relative density. This points to the fact that for the tensile loading case, stochastic structures are not able to surpass the cube edge. This points to the fact that a simple loading case such as tension a cube edge structure with struts in the same direction as the load is the optimum for stress distribution within the structure.

Observations for Torsional Loading Case

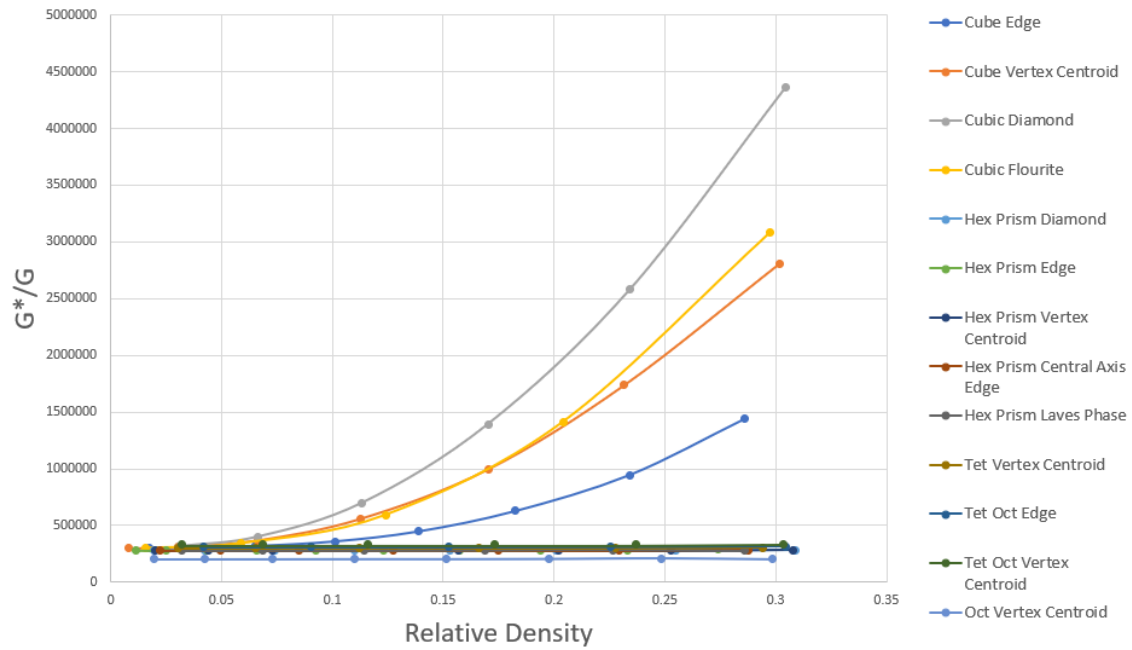


Figure 34- Relative shear modulus versus relative density plot for periodic shapes

The graph shown above was generated for all the periodic shapes over a range of relative density for the relative shear modulus (G^*/G). This plot shows that Cubic Diamond has the highest value of relative shear modulus over the lattice range of relative density of all the regular periodic shape lattices. The range of relative density is developed by varying the node thicknesses of the lattices in each case.

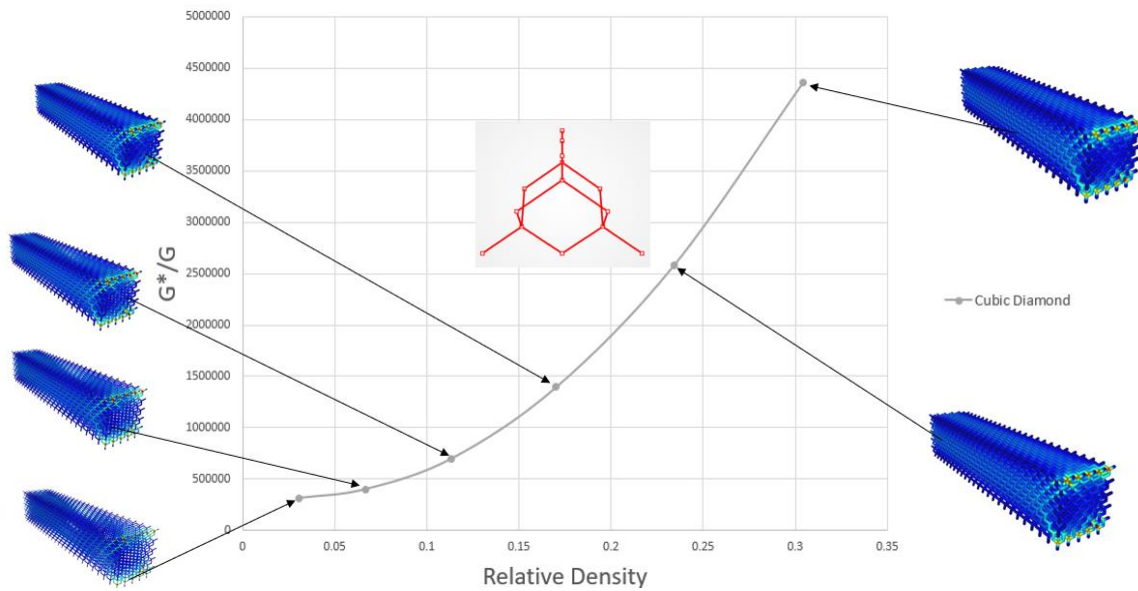


Figure 35- Relative shear modulus versus relative density plot and corresponding contour plots for Cubic Diamond

The above plot shows the relative Shear Modulus of Cubic Diamond over the range of lattice relative density. This plot also shows the stress contour plots for Cubic Diamond at different intervals of relative density. It can be seen that as the thickness and through that the relative density increases, the stress bearing capacity of the lattice also increases.

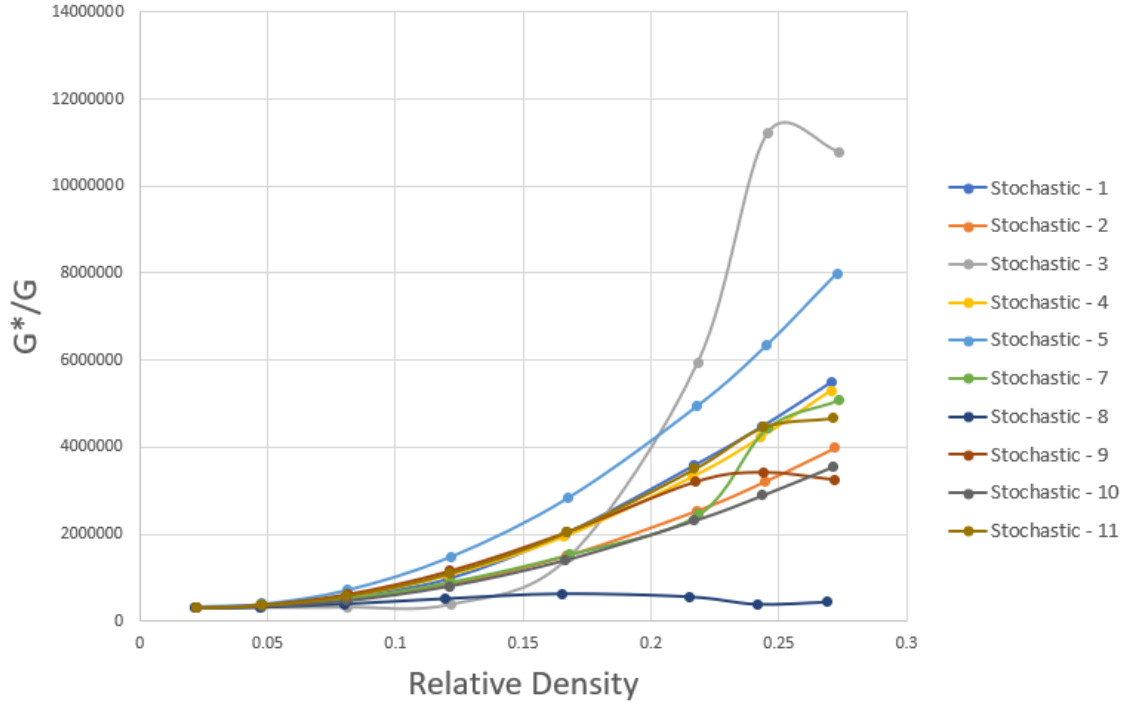


Figure 36- Relative shear modulus versus relative density plot for stochastic shapes

Next, the response of stochastic structures to tensile load was analyzed. For this, stochastic structures with different seed values from 1 to 11 were taken. These seed values were found to be ample for a complete analysis of the stochastic shapes under tensile loading.

When each of these shapes were plotted for their metric values versus the corresponding relative density, over the lattice density range, the plot shown above is observed. It can be seen that over the selected range of relative density, Stochastic Seed-5 has the highest value of relative Shear Modulus. It can be seen that Stochastic Seed-3 can also be considered as the shape with higher relative stiffness value at higher values of relative density. But since the behavior is not monotonically increasing (which is the

behavior of periodic shapes and Stochastic Seed-5), behavior of Stochastic Seed-3 has not been studied further.

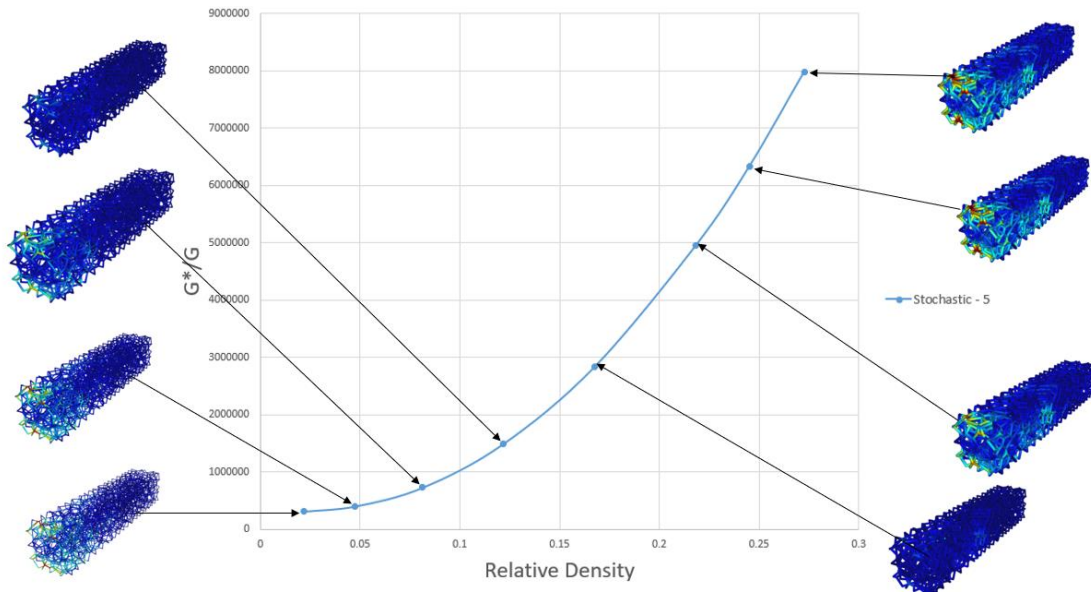


Figure 37- Relative shear modulus versus relative density plot and corresponding contour plots for Stochastic- Seed 5

The above plot shows the relative Shear Modulus of Stochastic-Seed 5 over the range of lattice relative density. This plot also shows the stress contour plots for Stochastic-Seed 5 at different intervals of relative density. It can be seen that as the thickness and through that the relative density increases, the stress bearing capacity of the lattice also increases.

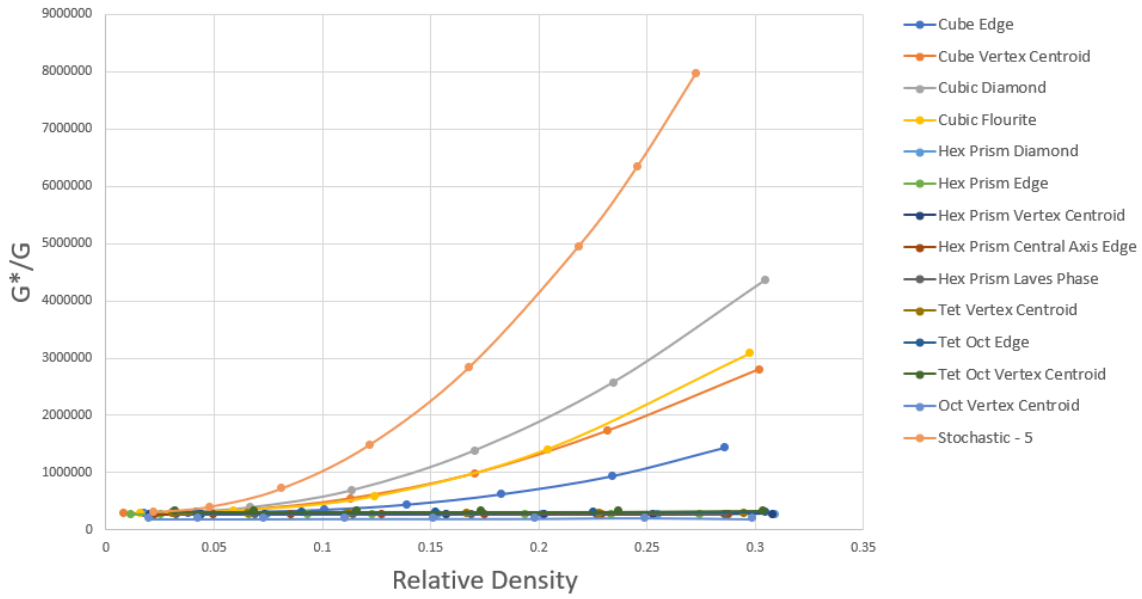


Figure 38- Relative shear modulus versus relative density plot for Stochastic-Seed 5 and periodic shapes

Stochastic Seed-1, the stochastic shape with the highest value of Shear rigidity was plotted along with the other periodic shape. As can be seen from the plot above, Stochastic Seed-1 has the highest value of relative bending rigidity when compared to all the periodic shapes over the entire range of lattice relative density. This points to the fact that for the torsional load case, stochastic structures have the potential to surpass periodic cell shapes.

Reproducibility of Simulation Results

In theory, the metrics selected to analyze the simulation results have been normalized for the choice of material. In order to verify this claim, the symmetric bending simulation analysis was performed in the same manner as performed earlier, the

only difference was that material Inconel 718 (Special Metals) was chosen instead of PA 2200. The motivation to choose Inconel 718 was the fact that it is one of the most common materials used in the metal additive manufacturing process of Laser Powder Bed Fusion (LPBF).

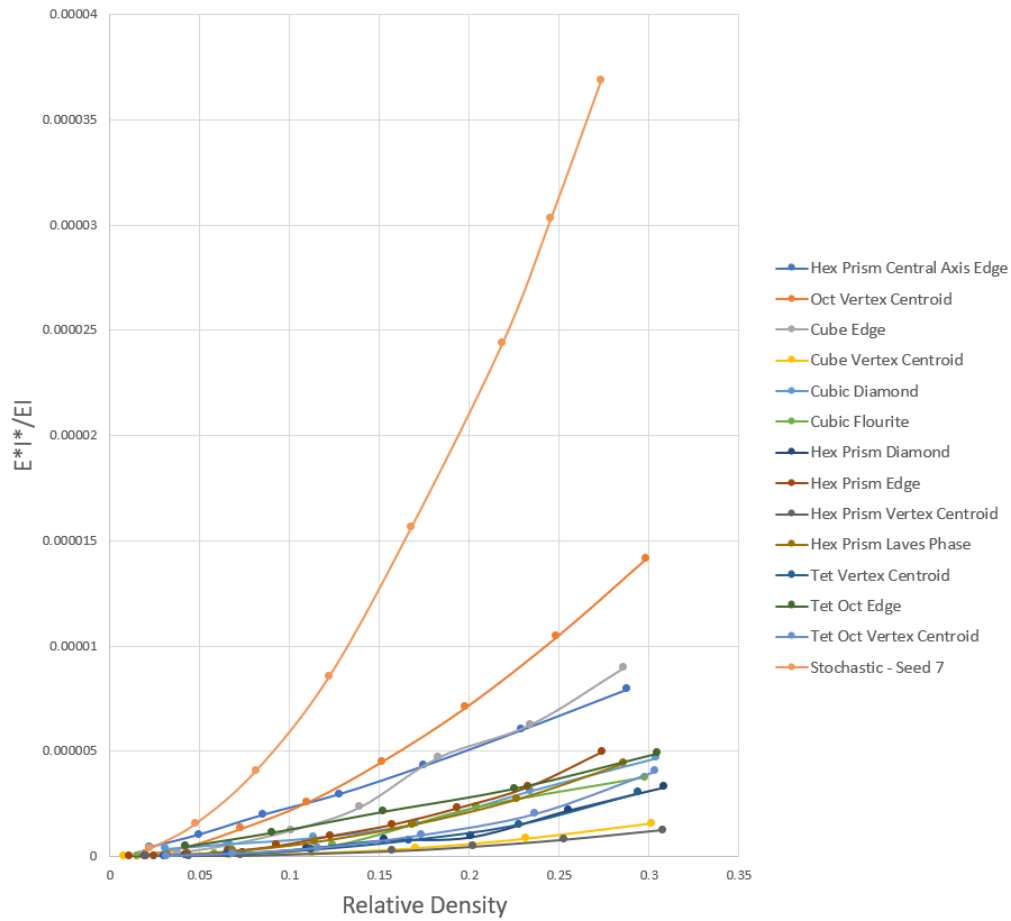


Figure 42- Relative bending rigidity versus relative density plot for Stochastic-Seed 7 and periodic shapes using Inconel 718

On comparing Figure 42 (symmetric bending results for Inconel 718) and Figure 31 (symmetric bending results for PA 2200) it can be seen that the trends as well as the numerical values are almost identical with minimum error for each of the shapes. This

provides testimony to the fact that results obtained numerically (computationally) for the same metric are not dependent on the choice of material. This reproducibility of results is expected in the case of tension and shear loading conditions as well.

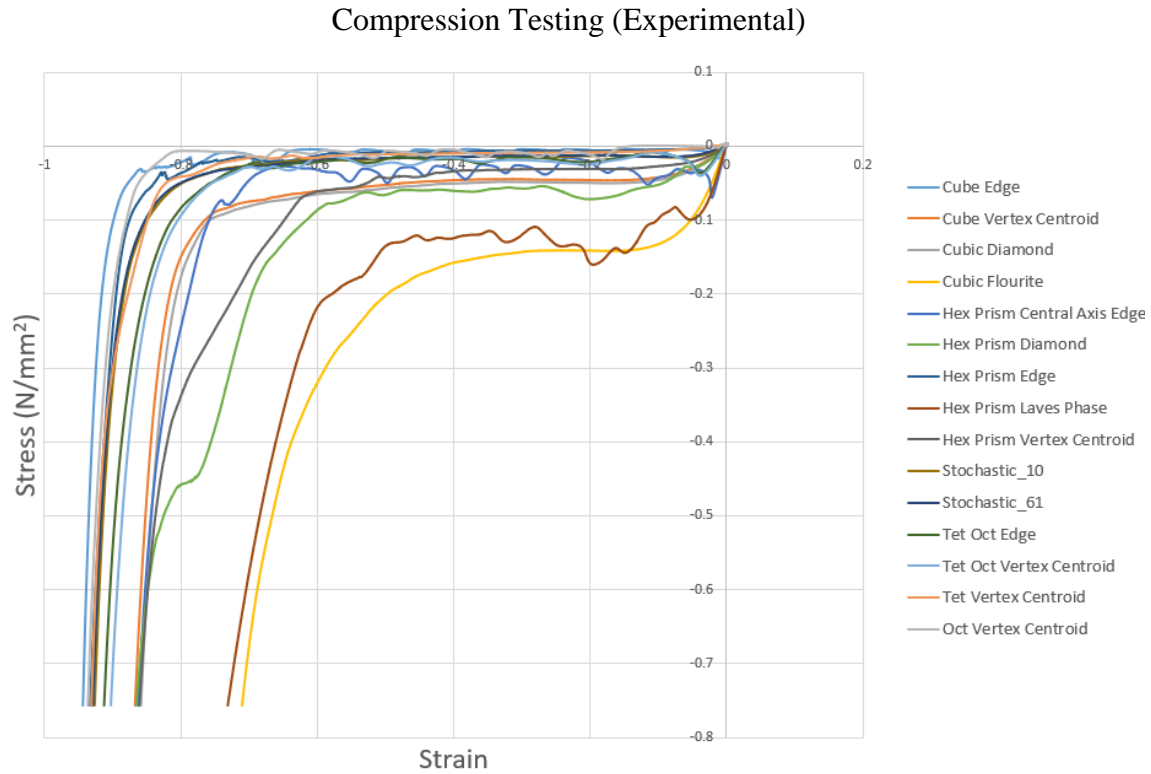


Figure 43- Stress vs strain curves for quasi-static compression after testing

The above figure shows the results of compression testing data collected for the testing of lattices consisting of 13 periodic shapes and two stochastic shapes. The Random Seed value for the Stochastic shapes is 10 and 61 respectively. All the specimens had the node thickness of 1mm. These testing curves are consistent with the behavior described by Ashby (Ashby 2006) for stretch dominated and bending dominated lattice structures.

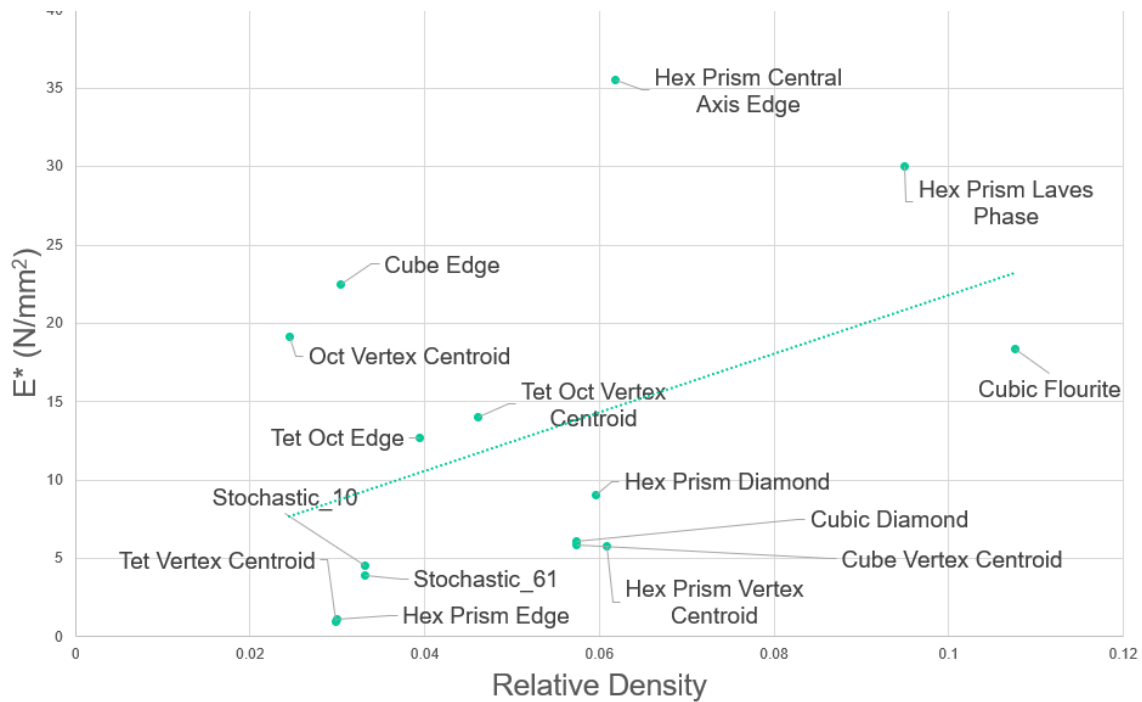


Figure 45- Young's modulus versus relative density scatter plot for tested specimen with linear fit

Figure 45 shows a scatter plot of the effective Young's modulus and relative density of the specimens with a linear fit. Linear fit provides a qualitative idea as to how well a shape is performing in terms of high stiffness. Shapes above the linear fit have higher stiffness as compared to those below it and higher the shape above the fit, stiffer it is. Also, the more a shape is on the left, the lighter it is for a given value of stiffness. Hence, higher and more to the left a shape is on the plot, more better performing the shape is in terms of high stiffness as a characteristic of its shape.

The effective modulus of the cube edge shape (23.61 N/mm^2) was compared with the simulation value (19.94 N/mm^2) of the same and it was found to be within an error of 12.74%.

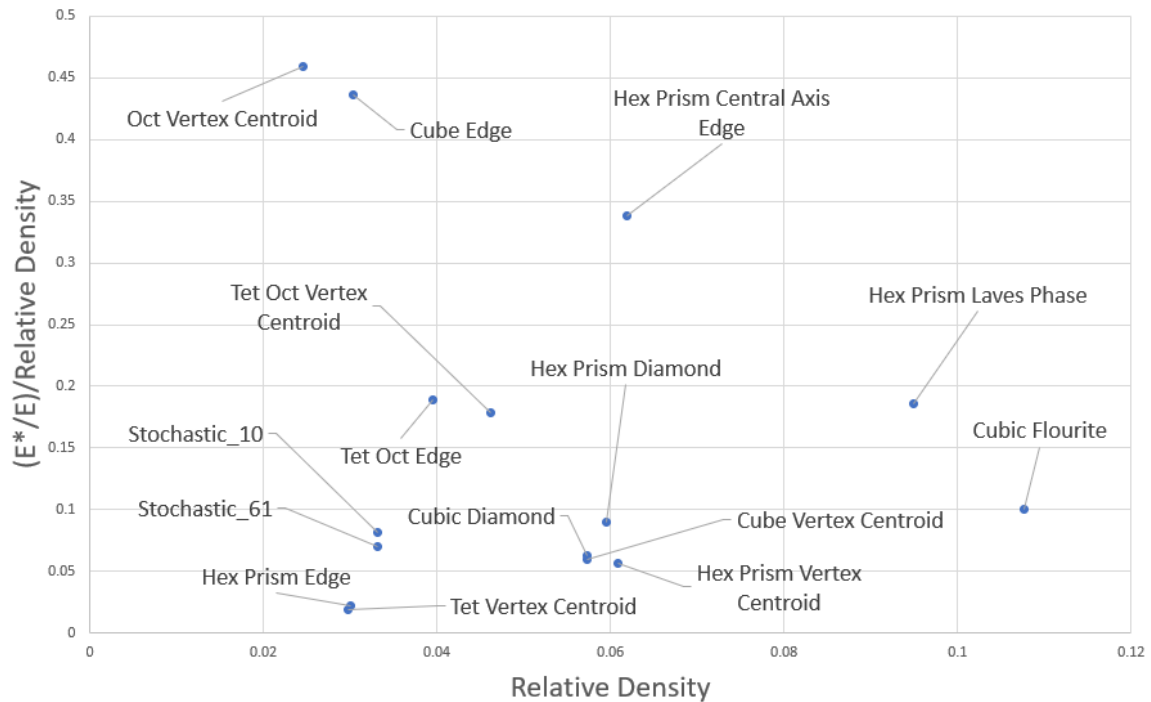


Figure 46- Relative young's modulus per unit relative density versus relative density scatter plot for the tested specimen

This is the experimental result with the relative density normalized. The further away a shape is placed, more is the stiffness of that shape under compression. From the plot it can be deduced that Oct Vertex Centroid lattice is the stiffest followed by Cube Edge. However, during manufacturing, the end plates did not bond properly for the Oct Vertex Centroid lattice hence there was not a proper transfer of load and the specimen was moving in the lateral direction during compression testing which means the data

collected for Oct Vertex Centroid lattice is unreliable. Hence, the second stiffest lattice, the Cube Edge lattice is in fact the stiffest which agrees with our simulation data.

DISCUSSION

Periodic Case: Bending

The relative bending rigidity plots generated from the computational data suggests that from the pool of arbitrarily chosen 13 open-celled regular shapes, the lattice of Oct Vertex Centroid shape has the highest value of relative bending rigidity as compared to the lattices of other cell shapes across the entire range of lattice relative density (0.01-0.3). The Tet Oct Edge lattice is the least stiff or most compliant to bending response. All the lattices of other periodic shapes lie in between these two extremes.

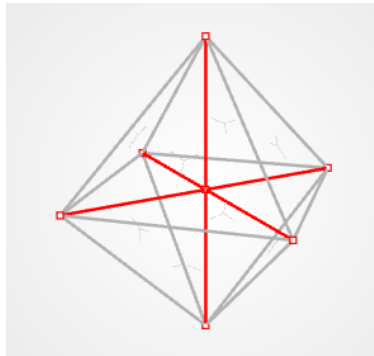


Figure 39- Oct Vertex Centroid unit cell

As can be seen from the unit cell, Oct Vertex Centroid has the nodal connectivity $Z=6$, which as per Maxwell's, criterion makes the lattice consisting of this structure

stretch-dominated and compared to bending dominated structures, (Deshpande, Ashby, and Fleck 2001) these are much stiffer by the virtue of just their configuration. This provides an analytical justification of sorts for high relative bending rigidity observed in Oct Vertex Centroid lattices.

Periodic Case: Tension

The relative Young's Modulus plots generated from the computational data suggests that from the pool of arbitrarily chosen 13 open-celled regular shapes, the lattice of Cube Edge shape has the highest value of relative Young's modulus as compared to the lattices of other cell shapes across the entire range of lattice relative density (0.01-0.3). The Tet Vertex Centroid lattice is the least stiff or most compliant to tension loading. All the lattices of other periodic shapes lie in between these two extremes.

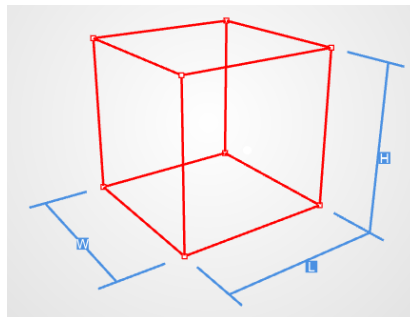


Figure 40- Cube Edge unit cell

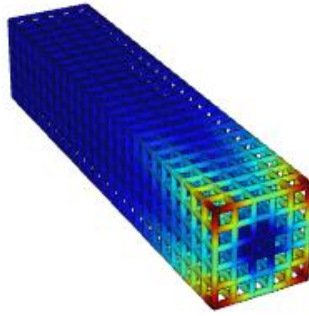


Figure 41- Cube Edge lattice with 1.6mm node thickness

As can be seen from the lattice and the unit cell, all the members are perpendicular to each other. There are long beams running in the axial direction of the lattice, which is same as the direction of the applied load. These structures are then reinforced with members in the perpendicular direction. Such an arrangement of beams allows for high load transfer from one end to the other, which reduces stress concentration at points where the load is applied, increasing the bearing strength of the structure.

Periodic Case: Torsion

The relative Shear Modulus plots generated from the computational data suggests that from the pool of arbitrarily chosen 13 open-celled regular shapes, the lattice of Cubic Diamond shape has the highest value of relative Shear modulus as compared to the lattices of other cell shapes across the entire range of lattice relative density (0.01-0.3). The Oct Vertex Centroid lattice is the least stiff or most compliant to torsional loading. All the lattices of other periodic shapes lie in between these two extremes.

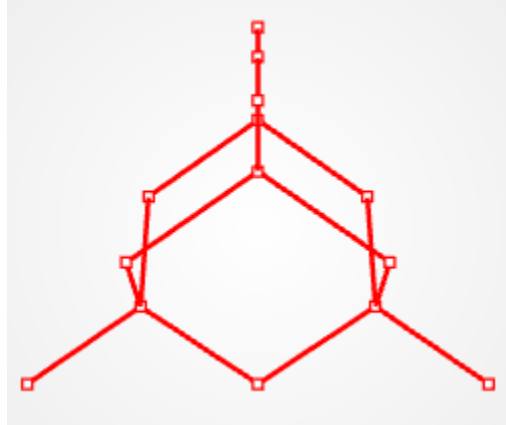


Figure 42- Cubic Diamond unit cell

Torsional load is a complex loading condition in the sense that direction of force keeps changing in the lateral plane as the load is applied. As can be seen from the unit cell, Cubic Diamond has struts or beams in-plane as well as out of plane and that too in multiple directions in a given plane. This allows the Cubic Diamond lattice to have load bearing members in different orientation of the lattice while the load is being applied which aids to the strength and ultimately shear stiffness of the lattice. As can be seen in Fig. 51 for the Cubic Diamond lattice, there is high load transfer of stress from the members to the load is applied to the very end of the lattice.

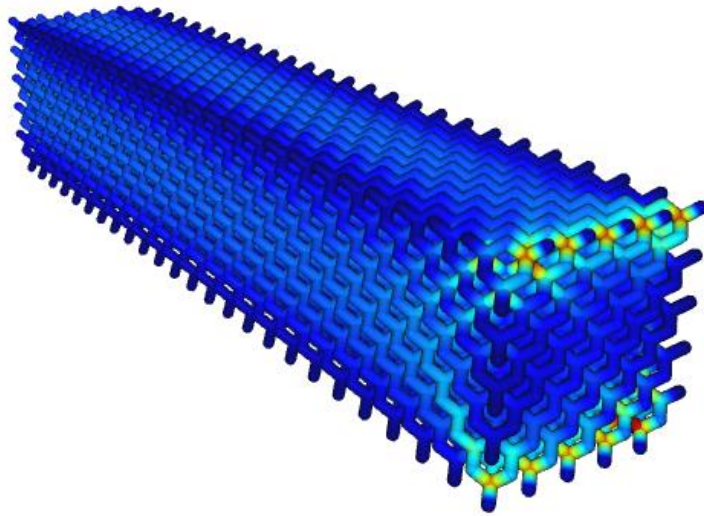


Figure 43- Cubic diamond lattice subjected to torsion

Stochastic Case: Bending

From the stochastic study and overall results from the bending loading case it can be concluded that Stochastic-Seed 7 is not only the stiffest relative rigidity case among the stochastic bodies but among all the periodic cases as well. While performing the stochastic analysis, configurations such as Stochastic-Seed11, which showed high compliance or low stiffness towards bending load were encountered. Also, there were some Stochastic structures which showed low stiffness to bending load at low relative densities and then their stiffness increases drastically (Stochastic-Seed3). Stochastic lattices which were non-monotonically increasing or decreasing in behavior during analysis, that is, they were showing behavior which was not comparable to the monotonically increasing behavior of periodic lattices, were not considered for an apt comparison.

Stochastic Case: Tension

From the stochastic study for the tensile loading case, it can be concluded that Stochastic Seed-4 is the stiffest tensile loading lattice among all the stochastic lattices and the second stiffest when compared to periodic lattices, Cube Edge Lattice being the stiffest. As with the bending loading case, there were some Stochastic structures which showed low stiffness to bending load at low relative densities and then their stiffness increases drastically (Stochastic-Seed1). Similar to the bending loading case, stochastic lattices which were non-monotonically increasing or decreasing in behavior during analysis, that is, they were showing behavior which was not comparable to the monotonically increasing behavior of periodic lattices, were not considered for an apt comparison.

Stochastic Case: Torsion

Similarly, from the stochastic study and overall results from the torsion loading case it can be concluded that Stochastic-Seed 5 is not only the stiffest relative rigidity case among the stochastic bodies but among all the periodic cases as well. While performing the stochastic analysis, configurations such as Stochastic-Seed11, which showed high compliance or low stiffness towards bending load were encountered. Also, there were some Stochastic structures which showed low stiffness to bending load at low relative densities and then their stiffness increases drastically (Stochastic-Seed 4). Stochastic lattices which were non-monotonically increasing or decreasing in behavior during analysis, that is, they were showing behavior which was not comparable to the

monotonically increasing behavior of periodic lattices, were not considered for an apt comparison.

From the study of stochastic specimens under the cases of bending, torsion and tension, it is can be seen that with the appropriate value of the ‘Random Seed’ which corresponds to a specific stochastic configuration, a large variety of design problems can be tackled. Not only classical design optimization problems such as maximizing stiffness, which was performed in this study, can be dealt with stochastic structures but also, complex problems which require highly non-monotonic behavior can utilize the mechanical properties of stochastic structures.

The methodology developed in this study for evaluating cell shapes, both periodic and stochastic, can be extended to cell shapes and lattice geometries not included in this study for the compliance minimization problem. A qualitative plot capturing the performance of shape lattices under all the three loading conditions as a function of minimum compliance is shown below:

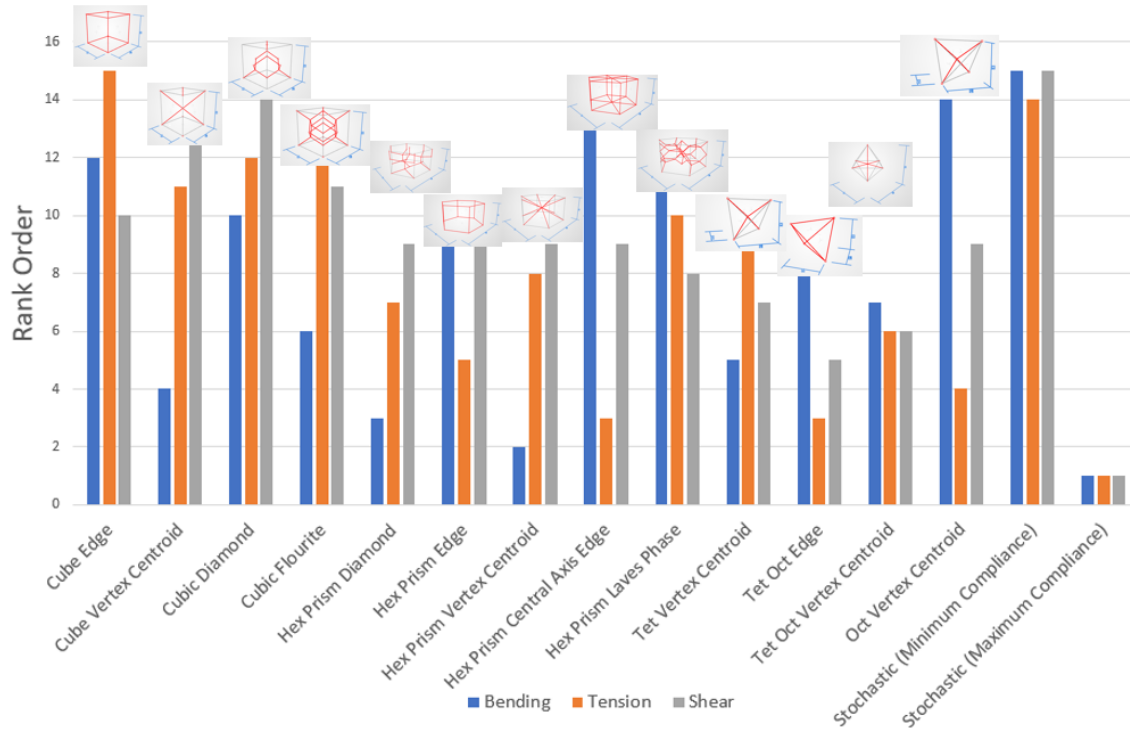


Figure 44- Qualitative histogram of various shapes evaluating stiffness metric under respective load cases

In this plot, the average value of the metric value of each shape under each loading condition was taken over the entire range of lattice relative density. Then these values were ranked from highest to lowest in order. Higher the rank of a shape, stiffer it is on an average for a given load case. To give a general idea to the potential of the versatility of stochastic design, stochastic shapes of minimum compliance and maximum compliance have also been ranked.

Effect of Node Thickness

One of the major effects that has not been captured effectively in the simulation results is the effect of node thickness. As stated and proven by Portela, (Portela, Greer, and Kochmann 2018) the increase in node thickness contributes to the increase in stiffness of a lattice when the ratio of the effective length of strut and the node radius is greater than 0.5. This effect is not captured by Element while calculating results.



Figure 53- No nodes after thickening of lattice by solver

The file generated by the solver is an ELEM file which is required to be converted to an STL file if the lattice is to be printed with an IGES file being the intermediate

medium CAD format for conversion. As can be seen from Figure 53, the lattice thickened by the solver has no nodes.

For file conversion, the Element solver generates nodes for the STEP file after the solution has been generated which means the effect of nodes wasn't captured in the calculations which makes node effect a major source of error in estimating stiffness.



Figure 54 – Nodes can be seen prominently in the CAD file (left) and printed sample (right) of Cube Edge lattice

From Figure 54 we can see that nodes are a prominent part of the geometry and play a decisive role in determining the behavior of the lattice under a given loading condition.

LIMITATIONS

The following limitations are identified pertaining to the work discussed here:

- For the pool of periodic unit cell shapes, only open-celled unit cells were chosen. This was done as the mechanics of open-celled unit cells is simpler to evaluate and evaluating closed-celled structures would have increased the number of shapes that have to be evaluated significantly and that would not have allowed timely completion of the research undertaken.
- Another limitation is the fact that all the computational as well as testing was done keeping the Nylon PA 2200 material in mind. Even though the computational results were normalized for material properties, but whether these results are truly reproduceable for another material is something that remains to be investigated.
- All simulation results presented here assume linear elastic behavior and are derived from static stress analyses. The experimental work in this study represents a preliminary investigation into what is otherwise largely a numerical study and was conducted with the intent of identifying what other considerations are important to the development of a usable analysis and prediction tool. More work is needed in this area to truly examine the validity of these simulation tools in the

real world and also to study the effect of material and manufacturing imperfections on their predictions.

CONCLUSIONS AND FUTURE WORK

This work of research was aiming to make a contribution to the first question of the four questions of lattice design (Bhate, 2019): what is the optimum cell shape for a specific application? Towards that end, this work has identified the following broad conclusions, summarized from the previous sections discussions:

- Selection methods based on unit cell approaches alone are likely to be sub-optimal since local stress distributions in a three-dimensional part can be more complex than pre-supposed in most unit-cell studies.
- A methodology that examines the performance of a structure under various loading conditions has been demonstrated as an alternative to unit cell based selection methods.
- The same periodic unit lattice shape that is optimal under one loading condition, may not be so under different loads.
- Stochastic structures with the “right” seed, can have interesting performances that exceed those of periodic structures in loading cases beyond the uniaxial.

Resulting from this work, some areas for future work are recommended:

- This work is merely an initiation point to answering the four questions of cellular design, which will ultimately allow to develop a novel design methodology for lattice design. More work is needed to address these questions.
- A somewhat unexpected observation from this investigation is that stochastic structures have a lot of potential for application specific structural design as long as they can be designed deterministically to select the optimal configurations. Further investigation into stochastic behavior that looks at the underlying reasons behind the mechanics of these structures and develops automated methods of evaluating them has the potential to further expand the impact of lattice materials.

BIBLIOGRAPHY

- Gibson, L. J., & Ashby, M. F. (1997). *Cellular Solids by Lorna J. Gibson*. Retrieved 6 12, 2019, from <https://cambridge.org/core/books/cellular-solids/bc25789552baa8e3cad5e1d105612ab5>
- Gibson, L. J., & Ashby, M. F. (1997). *Cellular Solids: The mechanics of honeycombs*. Retrieved 5 29, 2019, from <https://cambridge.org/core/books/cellular-solids/the-mechanics-of-honeycombs/fc24e44367416b6d277ba28d3678e301>
- Hibbeler, R. (2004). *Mechanics of Materials*. Pearson Education. Retrieved 6 9, 2019
- Bhate, Dhruv. "Four Questions in Cellular Material Design." *Materials (Basel, Switzerland)* 12.7 (2019): *Materials (Basel, Switzerland)*, March 31, 2019, Vol.12(7). Web.
- J.C. Maxwell, 1864, "On reciprocal figures and diagrams of forces", *Philosophical Magazine, vol 4, issue 27*, pages 250-261
- Maxwell, J. (1870). I.—On Reciprocal Figures, Frames, and Diagrams of Forces. *Transactions of the Royal Society of Edinburgh*, 26(1), 1-40. doi:10.1017/S0080456800026351
- Ashby, M.F., Evans, A.G., Fleck, N.A., Gibson, L.J., Hutchinson, J.W. & Wadley, H.N.G. 2000 *Metal foams: a design guide*. Oxford, UK: Butterworth:Heinemann
- Ashby, M.F. 2006. "The Properties of Foams and Lattices." *Philosophical Transactions of the Royal Society A: Mathematical, Physical and Engineering Sciences* 364(1838): 15–30.
- Berger, J. B., H. N.G. Wadley, and R. M. McMeeking. 2017. "Mechanical Metamaterials at the Theoretical Limit of Isotropic Elastic Stiffness." *Nature* 543(7646): 533–37.
- Bhate, Dhruv, Clint Penick, Lara Ferry, and Christine Lee. 2019. "Classification and Selection of Cellular Materials in Mechanical Design: Engineering and Biomimetic Approaches." *Designs* 3(1): 19.
- Deshpande, V S, M F Ashby, and N A Fleck. 2001. "FOAM TOPOLOGY BENDING VERSUS STRETCHING DOMINATED ARCHITECTURES." 49: 1035–40.
- Fleck, N. A., V. S. Deshpande, and M. F. Ashby. 2010. "Micro-Architected Materials : Past , Present and Future." (May): 2495–2516.
- Le, Thao, Dhruv Bhate, John M Parsey, and Keng H Hsu. 2017. "Determination of a Shape and Size Independent Material Modulus for Honeycomb Structures in Additive Manufacturing." *Solid Freeform Fabrication Symposium*.

- Meza, Lucas R. et al. 2017a. "Reexamining the Mechanical Property Space of Three-Dimensional Lattice Architectures." *Acta Materialia* 140: 424–32.
<https://doi.org/10.1016/j.actamat.2017.08.052>.
- Meza, Lucas R et al. 2017b. "Acta Materialia Reexamining the Mechanical Property Space of Three-Dimensional Lattice Architectures." *Acta Materialia* 140: 424–32.
<https://doi.org/10.1016/j.actamat.2017.08.052>.
- Pellegrino, S, and C R Calladine. 1986. "Matrix Analysis of Statically and Kinematically Indeterminate Frameworks." *International Journal of Solids and Structures* 22(4): 409–28. [http://dx.doi.org/10.1016/0020-7683\(86\)90014-4](http://dx.doi.org/10.1016/0020-7683(86)90014-4).
- Portela, Carlos M, Julia R Greer, and Dennis M Kochmann. 2018. "Impact of Node Geometry on the Effective Stiffness of Non-Slender Three-Dimensional Truss Lattice Architectures." *Extreme Mechanics Letters* 22: 138–48.
<https://doi.org/10.1016/j.eml.2018.06.004>.
- Rosen, David W., Scott Johnston, Marques Reed, and Hongqing Wang. 2006. "Design of General Lattice Structures for Lightweight and Compliance Applications." *Rapid Manufacturing Conference* (March): 1–14.
<http://smartech.gatech.edu/handle/1853/33037>.
- Seepersad, Carolyn Conner, Janet K. Allen, David L. McDowell, and Farrokh Mistree. 2006. "Multifunctional Topology Design of Cellular Material Structures." *Volume 1: 32nd Design Automation Conference, Parts A and B* 2006: 499–513.
<http://proceedings.asmedigitalcollection.asme.org/proceeding.aspx?articleid=1588141>.
- Sharma, Nitin, Ronald F. Gibson, and Emmanuel O. Ayorinde. 2006. "Fatigue of Foam and Honeycomb Core Composite Sandwich Structures: A Tutorial." *Journal of Sandwich Structures and Materials* 8(4): 263–319.
- Sharma, Raghav et al. 2018. "A Comparison of Modeling Methods for Predicting the Elastic-Plastic Response of Additively Manufactured Honeycomb Structures." In , 791–807.
- V, George; Nader Engheta. 2011. "Metamaterials : Fundamentals and Applications in the Microwave and Optical Regimes." *proceedings of the IEEE* 99(10): 1618–21. ???
- Wei, Kai, Haosen Chen, Yongmao Pei, and Daining Fang. 2016. "Planar Lattices with Tailorable Coefficient of Thermal Expansion and High Stiffness Based on Dual-Material Triangle Unit." *Journal of the Mechanics and Physics of Solids* 86(December): 173–91. <http://dx.doi.org/10.1016/j.jmps.2015.10.004>.
- Zhu, Mengke, and Tony S. Keller. 2004. "Mechanical Properties of Cellular Materials." *Journal of Biomechanics* 25(6): 662.
- Electro Optical Systems. *Material Data Sheet, PA 2200*.
- Special Metals. *Material Data Sheet, Inconel alloy 718*.

- Medikonda, Sandeep. “ANSYS Material Designer”,
<https://studentcommunity.ansys.com/thread/material-designer-introduced-in-19-2/>. 4 October 2018.
- “Autodesk Netfabb”. *Autodesk Inc.*
<https://www.autodesk.com/products/netfabb/features/simulation>. Accessed 25 May 2019
- Bagchi, Shibai. “What’s new in Generate for Windows”,
<https://www.frustum.com/frustum-resources/whats-new-in-generate-for-windows>.
Accessed: 25 May 2019
- “Introductory Webinar for Altair Optistruct”., *Altair Engineering Inc.*,
<https://web.altair.com/optistruct-revolutionizes-lattice-structures-for-3d-printing-0?submissionGuid=81efc8a0-96a8-445f-827f-1e61047dbda7>. Accessed 25 May 2019
- Bogomolny, Michael. “ParaMatters – Generative Design for Engineering”,
<https://www.linkedin.com/in/michael-bogomolny-ph-d-95636499/detail/recent-activity/posts/>. 24 June 2018
- “IntraLattice Documentation”., *ADML Labs, McGill University, Canada.*,
<http://intralattice.com/userdocs>. Accessed 24 June 2019
- “Simpleware for 3D printing”., *Synopsys Inc.*,
<https://www.synopsys.com/simpleware.html>. Accessed 24 May 2019
- “Stochastic Distribution and Seeds”., *Eindhoven University of Technology.*
<http://cif.se.wtb.tue.nl/tools/cif3sim/distr-seeds.html>, Accessed 10 May 2019